

The aim of the present work is to determine accurate metallicities for a group of red giant branch stars in the field of the bulge Globular Cluster NGC 6441. This is the third paper of a series resulting from a large project aimed at determining the extent of the Na-O anticorrelation among Globular Cluster stars and exploring its relationship with HB morphology. We present an LTE abundance analysis of these objects, based on data gathered with the FLAMES fiber facility and the UVES spectrograph at VLT2. Five of the thirteen stars observed are members of the cluster. The average Fe abundance for these five stars is $[\text{Fe}/\text{H}] = -0.39 \pm 0.04 \pm 0.05$ dex, where the first error bar includes the uncertainties related to star-to-star random errors, and the second one the systematic effects related to the various assumptions made in the analysis. The overall abundance pattern is quite typical of Globular Clusters, with an excess of the α -elements and of Eu. There is evidence that the stars of NGC 6441 are enriched in Na and Al, while they have been depleted of O and Mg, due to H-burning at high temperatures, in analogy with extensive observations for other Globular Clusters: in particular, one star is clearly Na and Al-rich and O and Mg-poor. We obtained also quite high V abundances, but it is possible that this is an artifact of the analysis, since similar large V abundances are derived also for the field stars. These last are all more metal-rich than NGC 6441 and probably belong to the bulge population.

Key words. Stars: abundances - Stars: atmospheres - Stars: Population II - Galaxy: Globular Clusters: general - Galaxy: Globular Clusters: individual: NGC 6441

Na-O Anticorrelation And HB. III. The abundances of NGC 6441 from FLAMES-UVES spectra [★]

R.G. Gratton¹, S. Lucatello¹, A. Bragaglia², E. Carretta², Y. Momany^{1,3}, E. Pancino², E. Valenti^{2,4}

¹ INAF-Osservatorio Astronomico di Padova, Vicolo dell'Osservatorio 5, 35122 Padova, ITALY

² INAF-Osservatorio Astronomico di Bologna, Via Ranzani 1, 40127 Bologna, ITALY

³ Dipartimento di Astronomia, Università di Padova, Vicolo dell'Osservatorio 5, 35122 Padova, ITALY

⁴ Dipartimento di Astronomia, Università di Bologna, Via Ranzani 1, 40127 Bologna, ITALY

Received: ; accepted:

Abstract.

1. Introduction

NGC 6441 is a very luminous ($M_V = -9.18$: Harris 1996) and massive Globular Cluster located in the inner regions of our Galaxy: according to Harris (1996) it is located about 2.1 kpc from the Galactic center on the other side of the Galaxy with respect to the Sun. NGC 6441 has raised a considerable interest because, in spite of being a metal-rich cluster ($[Fe/H] = -0.53 \pm 0.11$, Armandroff & Zinn 1988), it has a very extended horizontal branch, with several stars on the blue side of the instability strip (Rich et al. 1997). Layden et al. (1999) estimated that about 17% of the horizontal branch stars are found in a feature bluer and brighter than the red clump, a peculiarity shared with the other massive, metal-rich bulge cluster NGC 6388 (Rich et al. 1997). NGC 6441 has also a quite rich and peculiar population of RR Lyrae (Layden et al. 1999; Pritzl et al. 2001), characterized by long periods in spite of the high metallicity of the Cluster. The color-magnitude diagram of NGC 6441 presents other peculiarities: the red giant sequence is broad, and the clump is clearly tilted. These features may at least in part be justified by differential reddening (see e.g. Layden et al. 1999). However, given that NGC 6441 is bright and massive, some star-to-star spread in the metal abundances cannot be excluded. Such a possibility was raised in order to explain the odd properties of the horizontal branch and of the RR Lyrae population (Piotto et al. 1997; Sweigart 2001; Pritzl et al. 2001); however, very recently Clementini et al. (2005) have shown that most of the RR Lyrae of NGC 6441 are metal-rich, likely in accordance to the other cluster stars.

The peculiarities of NGC 6441 must then still find a comprehensive explanation.

All the previous discussion seems to imply that NGC 6441 is further evidence of the second parameter effect in Globular Clusters; here, like in NGC 2808, the second parameter effect is manifest within the same cluster. A peculiarity of NGC 6441 (and of NGC 6388) is that the blue horizontal branch is brighter than the red one. This might be explained by a higher content in Helium (Sweigart & Catelan 1998). The existence of He-rich populations have been recently proposed to justify various features of some Globular Clusters (D'Antona & Caloi 2003; Bedin et al. 2004; Piotto et al. 2005; D'Antona et al. 2005). In particular, a He-rich population might indicate a second generation of stars born from the ejecta of the most massive of the intermediate-mass stars of the earlier generation, required to explain the observations of O-Na and Mg-Al abundance anticorrelations, ubiquitous in Globular Clusters but not observed among field stars (see the review by Gratton et al. 2004). If this scenario is correct, there should be a correlation between the distribution of the O/Na abundance ratios, observed e.g. on the red giant branch of a cluster, and the color distribution of stars along the horizontal branch of the same cluster.

In order to explore whether such a correlation indeed exists, we have undertaken an extensive spectroscopic survey of Globular Cluster stars with the FLAMES multi-fiber facility at ESO (Pasquini et al. 2002). With its high multiplexing capabilities, FLAMES can get spectra of hundreds of stars in Globular Clusters within a few hours of VLT observing time. FLAMES may simultaneously feed two spectrographs: GIRAFFE, which is most suited for observation of extensive samples of stars in restricted wavelength regions, and UVES, which provides extensive spectral coverage for a few stars. The latter

Send offprint requests to: R.G. Gratton

[★] Based on data collected at the European Southern Observatory with the VLT-UT2, Paranal, Chile (ESO 073.D-0211)

higher resolution ($R \simeq 40,000$) spectra may be used to carefully derive the chemical composition of the cluster, and possibly discover the existence of peculiarities due to its chemical evolution history, by comparing the abundance pattern with that obtained for field stars of similar characteristics.

NGC 6441 was an obvious candidate to be included in our sample. In this paper, we present an analysis of the FLAMES+UVES data we gathered for stars in this cluster, as well as for a few stars in the same field that turned out not to be members of the cluster. A separate paper will be devoted to the discussion of the GIRAFFE data.

2. Observations

Data used in this paper are based on exposures obtained in July 2004 with FLAMES at Kueyen (=VLT2) used in service mode. Details of the observations are given in Table 1.

NGC 6441 is a quite far and concentrated cluster ($c = 1.85$: Harris 1996) lying in a very crowded region, close to the direction of the Galactic center ($l = 353.53^\circ$, $b = -5.01^\circ$). Unluckily, when we started our project there was no suitable membership study available. These facts made identification of stars appropriate for abundance analysis difficult, given the safety constraints on fiber-to-fiber separation of the Oz-Poz FLAMES fiber positioner, and the need to avoid stars whose images are blended with neighbors. Our targets were carefully selected from high quality photometry.

The photometric data have been obtained within the observing program 69.D-0582(A) on June 2002 at the 2.2 m ESO/MPI telescope at La Silla Observatory (Chile), using the optical camera WFI. The exceptional capabilities of this imager provide a mosaic of eight CCD chips, each with a field of view of $\sim 8' \times 16'$, for a total field of view of $\sim 34' \times 33'$. The cluster center was roughly centered on Chip #7, and the images were taken through the V and I_c broad band filters with typical exposure times of 80 sec and 50 sec, respectively. During the night the average seeing was quite good (full width half maximum $\text{FWHM} \approx 0''.9$).

Stellar photometry was performed using the standard and tested DAOPHOT II and ALLFRAME programs (Stetson 1994). In crowded fields such as that surrounding NGC 6441, these programs provide high quality stellar photometry by point spread function (PSF) fitting (see Momany et al. 2002, 2004). The single PSFs were constructed for each image after a careful selection of isolated and well-distributed stars across each chip. The instrumental PSF magnitudes of NGC 6441 were normalized to 1 s exposure and zero airmass, and corrected for the aperture correction. The aperture corrections are necessary to convert the instrumental profile-fitting magnitudes of NGC 6441 on the scale of the standard star measure-

ments (based on aperture photometry, see below). The instrumental NGC 6441 magnitudes are therefore:

$$m' = m_{\text{apert.}} + 2.5 \log(t_{\text{exp}}) - K_\lambda X \quad (1)$$

where $m_{\text{apert.}} = m_{\text{PSF}} - \text{apert. correction}$, X is the airmass of the reference image for each filter, and the adopted mean extinction coefficients for La Silla are: $K_V = 0.16$ and $K_I = 0.07$. The aperture corrections were estimated upon isolated bright stars, uniformly distributed across the chip. For these we obtained aperture photometry after subtracting eventual nearby companions within 5 FWHM. The aperture magnitudes measured in circular apertures of 6 arcseconds in radius (close to the photoelectric aperture employed by Landolt 1992) were then compared to the PSF magnitudes, and the difference is assumed to be the aperture correction to apply to the PSF magnitudes.

Separately, aperture magnitudes of standard stars from 3 Landolt (1992) fields were measured in circular apertures of 6 arcseconds in radius. These aperture magnitudes were normalized to their corresponding airmass and exposure times, and compared with those tabled in Landolt (1992). A least square fitting procedure provided the calibration relations. The *r.m.s.* scatter of the residuals of the fit (0.009 and 0.011) are assumed to represent our calibration uncertainties in V and I respectively. The total zero-point uncertainties, including the aperture corrections and calibration errors, are 0.013, and 0.016 mag in V and I respectively. The PSF photometry of NGC 6441 (normalized and corrected for aperture correction) was then calibrated using the relations:

$$V = v' - 0.077(V - I) + 24.199 \quad (2)$$

$$I = i' + 0.097(V - I) + 23.142 \quad (3)$$

The *Guide Star Catalog (GSCII)* was used to search for astrometric standards in the entire WFI image field of view. Several hundred astrometric *GSCII* reference stars were found in each chip, allowing us an accurate absolute positioning of the sources. An astrometric solution has been obtained for each of the eight WFI chips independently, by using suitable catalog matching and cross-correlation tools developed at the Bologna Observatory. At the end of the entire procedure, the *rms* residuals are $\leq 0''.2$ both in right ascension and declination.

Only uncrowded stars were considered as possible targets, that is stars not showing any companion brighter than $V_{\text{target}} + 2$ mag within a 2.5 arcsec radius, or brighter than $V_{\text{target}} - 2$ mag within 10 arcsec. The targets were selected to lie close to the cluster mean locus in the color-magnitude diagram.

The fibers feeding the UVES spectrograph were centered on stars close to the tip of the RGB ($15.8 < V < 16.3$; see Figure 1). We used two different fiber configurations: in the first set, we observed six stars, with two fibers dedicated to the sky; in the second one, seven fibers were used for the stars, and one for the sky. The spectra cover the wavelength range 4700-6900 Å, and have $35 < S/N < 85$ for the combined exposures.

Table 1. Journal of observations

Fiber Configuration	Date	Time (UT)	Exp. Time (sec)	Seeing (arcsec)	Airmass
#1	2004-07-06	04:21:42	5300	1.59	1.040-1.174
	2004-07-11	02:48:19	5300	1.35	1.029-1.052
	2004-07-11	04:19:18	5300	0.91	1.055-1.221
#2	2004-07-17	05:18:20	5300	0.69	1.202-1.605
	2004-07-26	03:39:54	5300	1.04	1.077-1.282

As part of the service mode observations, the spectra were reduced by ESO personnel using the dedicated UVES-FLAMES pipeline (uves/2.1.1 version). We found that this UVES pipeline does not accurately subtract the background between orders in the green-yellow part of the spectra. Luckily, the redder part of the spectra included enough lines for our purposes. We hence relied on these pipelines reductions; the bluer portions of the spectra were then not considered in the present analysis.

3. Cluster membership

Table 2 gives details on the main parameters for the observed stars, providing for each one of them the distance in arcsec from the cluster center, the magnitudes, mean radial velocities, signal-to-noise ratios of the combined spectra and the σ of the EWs residuals, as well as the derived metallicity. Star designations are according to Valenti et al. (2006), from which photometric data were also taken. Coordinates (at J2000 equinox) are from our astrometry (Valenti et al. 2006); distances from the cluster center were obtained considering the nominal position given by Harris (1996). Radial velocities were measured from our spectra, using typically about 100 atomic lines. Errors in these velocities should typically be of a few hundreds of m/s. The signal-to-noise ratio S/N was estimated from the pixel-to-pixel scatter in spectral regions free from absorption lines at about 6200 Å.

Four of the thirteen observed stars (#7004050, 7004434, 7004463, and 7004487) are very likely members of the cluster, on the basis of the following criteria:

- they are projected close to the nominal cluster center, as given by Harris (1996). These four stars are the closest in our sample to the nominal cluster center, and are all within 150 arcsec from this position. Note that according to Harris (1996) the core radius of NGC 6441 is about 7 arcsec, and the tidal radius is about 467 arcsec.
- their radial velocities (+24.9, +13.6, +11.6, and +32.3 km s⁻¹ for stars 7004050, 7004434, 7004463, and 7004487, respectively) are close to the average radial velocity listed by Harris (+16.4 ± 1.2 km s⁻¹). The average velocity given by these four stars is +20.6 ± 4.9 km s⁻¹ (*r.m.s.* scatter of 9.8 km s⁻¹), in good agreement with the value listed by Harris.
- additionally, the four stars are confined in a very small range of colors, with 2.088 < $V - I$ < 2.168, with re-

spect to the rather broad color distribution along the apparent RGB of NGC 6441 (see Figure 1). This by itself is not a strong membership criterion, since the interstellar reddening is expected to be quite variable over the field (see Layden et al. 1999 for an extensive discussion). However, the close agreement between the colors of the confirmed member stars might indicate that differential reddening is less of a problem than expected, at least for these particular stars (it should be noted that all these stars are in the south-east quadrant of the cluster, quite close to each other).

- a posteriori, our analysis indicates that these stars have quite similar chemical composition. Again, this is not by itself a strong membership criterion, since there might be some spread in metallicity amongst the stars of NGC 6441 and because their metallicity is not unusual for bulge or disk field stars.

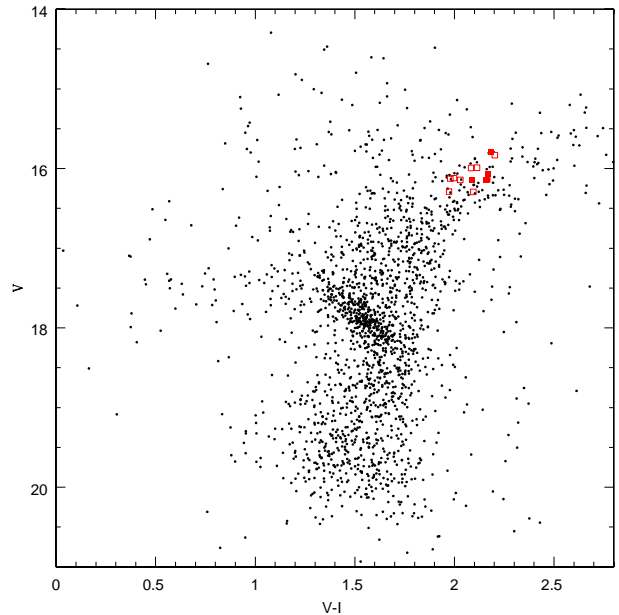


Fig. 1. $(V, V - I)$ color magnitude diagram for selected stars in the field of NGC 6441 (from Valenti et al. 2006). Large symbols are stars observed with UVES FLAMES. Filled symbols mark stars member of the cluster, on the basis of radial velocities and location in the field close to the cluster center; open symbols are non-member stars.

Table 2. Photometry and spectroscopic data for stars observed with UVES

Star	Fiber Conf.	RA (degree)	Dec. (degree)	Dist. (arcsec)	V (mag)	V-I (mag)	V-K (mag)	RV (km s ⁻¹)	S/N	σ (EW) (mÅ)	[Fe/H]	Notes
6003734	1	267.422	-36.9533	518	15.992	2.083	4.574	+83.5	39	8.7	-0.25	
6004360	2	267.475	-37.1471	414	16.127	1.979	4.403	+89.7	37	8.1	0.27	
6005308	1	267.463	-37.0816	284	16.290	1.973		-144.1	36	8.5	-0.17	
6005341	2	267.447	-36.9682	429	16.294	2.095	4.543	-41.2	50	9.4	0.06	
7003717	2	267.593	-36.9987	219	15.989	2.113	4.522	-134.0	50			fast rot.
7004050	1	267.543	-37.0793	106	16.062	2.168	4.775	+24.9	52	8.0	-0.45	member
7004329	1	267.581	-37.1614	404	16.120	1.997	4.258	-23.1	51	10.0	0.12	
7004434	2	267.541	-37.0849	127	16.142	2.167	4.719	+13.6	53	10.0	-0.34	member
7004453	1	267.525	-37.0109	167	16.144	2.029	4.382	-49.3	49	6.7	-0.04	
7004463	2	267.506	-37.0572	140	16.146	2.160		+11.6	77	9.1	-0.38	member
7004487	2	267.520	-37.0535	99	16.150	2.088	4.552	+32.3	82	6.1	-0.50	member
8002961	2	267.670	-37.0725	342	15.798	2.185	4.803	+54.1	86	5.8	-0.28	member?
8003092	1	267.753	-37.0622	573	15.832	2.203	4.923	-53.0	37	7.8	-0.25	

Among the remaining stars, #8002961 is also a possible cluster member, essentially on the basis of the not too large difference between its radial velocity (+54.1 km s⁻¹) and that of the cluster¹, and its location in the color magnitude diagram, since it lies close to the position occupied by the member stars. This star is projected at a quite large distance from the cluster center (341 arcsec), however still well within the tidal radius of NGC 6441. A posteriori, also the chemical composition supports cluster membership. It is noteworthy that the inclusion or exclusion of this particular stars from the group of objects considered cluster members does not affect our conclusions.

All remaining stars are unlikely to be cluster members, because of their discrepant radial velocities, large projected distances from the cluster center, much bluer colors, and often quite discrepant chemical composition. The rather large fraction of non-members did not come as a surprise, given the difficulties in identifying good candidates in this cluster and the strong contamination by field bulge stars. We notice that only observations by means of a multi-object facility like FLAMES could ensure the success of the program.

There are various circumstantial arguments that favor the membership to the bulge of all remaining stars. Three of them (#6005341, 7004329, and 7004453) have small negative radial velocities (-41.2, -23.1, and -49.3 km s⁻¹, respectively) and nearly solar Fe abundance. However, given the location of NGC 6441 at $b = -5.01$, they should be within 2-3 kpc from the Sun to be members of the thin disk (i.e. at no more than 200-300 pc from the galactic plane: see e.g. Bilir et al. 2005). Were this the correct distance of the stars, they would be subgiants, with a surface gravity of about $\log g \sim 3^2$. This

¹ While the velocity difference might appear large we note that NGC 6441 is well known to have an extremely large central velocity dispersion (around 17 km s⁻¹ see e.g. Dubath et al. 1997).

² This combination of effective temperatures and surface gravity would also be unlikely by evolutionary considerations,

is clearly excluded by their spectra, that indicate a much lower surface gravity of $\log g < 2$. These stars are then at more than 6 kpc from the Sun, and at more than 500 pc from the galactic plane. The same surface gravity argument can be applied to the remaining stars. We also note that stars #6003734 and #8003092 have a chemical composition similar to that of NGC 6441, but have very different radial velocities (+83.5 and -53.0 km s⁻¹) and are projected far from the cluster center (518 and 573 arcsec respectively, more than the tidal radius). Also star #6003734 is distinctly bluer than the cluster members considered above, while star #8003092 has magnitude and color very similar to those of star #8002961, that we considered a possible member. Star #6005308 has a chemical composition similar to that of NGC 6441: however its radial velocity is very different (-144.1 km s⁻¹), clearly incompatible with membership. Finally, star #6004360 has a large positive velocity of 89.7 km s⁻¹ and a large metal content. All these stars are distinctly bluer than the cluster members, although more metal-rich. This might be due to one of these three causes: smaller interstellar reddening (however there is no clear indication of this from our analysis); shorter distances (putting the stars close to the galactic center), or younger ages. As we will see, a shorter distance by about 20% is also suggested by the equilibrium of ionization. We conclude that all these stars most likely belong to the bulge population.

Finally, one of the target stars (#7003717) turned out to have very broad lines, likely widened by rotation. We measured a large negative radial velocity (-134.0 km s⁻¹), with clear indications of quite large variations over the small temporal range covered by our observations. Due to difficulties in the analysis, we did not further consider this star.

since subgiants are much warmer than ~ 4000 K for any reasonable chemical composition. Only pre-main sequence stars could occupy a similar location on the color-magnitude diagram

Table 3. Equivalent Widths from UVES spectra for the cluster members (in electronic form)

El.	Wavel. (Å)	E.P. (eV)	log gf	4050 EW (mÅ)	log A	4434 EW (mÅ)	log A	4463 EW (mÅ)	log A	4487 EW (mÅ)	log A	2961 EW (mÅ)	log A
Oi	6300.31	0.00	-9.75	56.2	8.23	83.9	8.61			63.4	8.45	68.7	8.39
Oi	6363.79	0.02	-10.25	29.7	8.44	50.9	8.76	15.8	8.14	38.5	8.65	33.3	8.44
Nai	6154.23	2.10	-1.57	99.4	6.36	105.4	6.14	140.8	6.62	100.4	6.20	110.5	6.34
Nai	6160.75	2.10	-1.26	111.1	6.25	137.5	6.24	154.4	6.49	123.3	6.19	136.2	6.40
Mgi	6318.71	5.11	-1.94	59.1	7.30	73.9	7.38	61.7	7.20	75.1	7.41	77.8	7.51
Mgi	6319.24	5.11	-2.16	48.2	7.31	64.6	7.46	48.5	7.22	53.0	7.29	70.8	7.61
AlI	6696.03	3.14	-1.32	99.9	6.30	128.3	6.40	164.2	6.95	106.6	6.22	127.4	6.54
AlI	6698.67	3.14	-1.62	77.7	6.18	92.4	6.18	119.9	6.62	71.1	6.00	89.4	6.21
SiI	5948.55	5.08	-1.23	67.7	7.41	85.4	7.47	103.0	7.75	84.4	7.44	84.4	7.57
SiI	6125.03	5.62	-1.57							27.9	7.35		
SiI	6145.02	5.62	-1.49			27.8	7.33	34.4	7.48	36.2	7.47	45.4	7.78
CaI	5857.46	2.93	0.24	164.0	5.75	178.9	5.55	207.6	5.88	169.2	5.63	175.7	5.70
CaI	5867.57	2.93	-1.49	56.5	5.59	77.5	5.74	92.8	6.01	69.9	5.76	77.4	5.82
CaI	6161.30	2.52	-1.27	109.0	5.88	141.1	5.89			135.4	6.03	144.7	6.16
CaI	6166.44	2.52	-1.14	103.8	5.64					136.5	5.92	136.0	5.89
CaI	6169.04	2.52	-0.80	145.2	6.02	158.1	5.69	169.9	5.90	160.5	5.95	156.9	5.89
CaI	6169.56	2.52	-0.48	136.7	5.58	176.2	5.62	187.9	5.80	146.2	5.42	169.4	5.74
CaI	6439.08	2.52	0.39	192.1	5.48	252.0	5.63	241.6	5.58	202.6	5.36	239.7	5.68
CaI	6455.60	2.52	-1.29	93.5	5.56	145.4	5.98	137.2	5.89	114.3	5.68	125.6	5.85
CaI	6462.57	2.52	0.26	246.0	5.99	309.9	6.12	296.6	6.08	261.3	6.00	280.9	6.07
CaI	6471.67	2.52	-0.69	140.9	5.93	194.2	6.11	162.7	5.72	158.4	5.85	173.9	6.08
CaI	6493.79	2.52	-0.11	166.6	5.72	209.8	5.73	209.7	5.77	180.5	5.59	198.8	5.82
CaI	6499.65	2.52	-0.82	113.4	5.56	176.3	5.99	163.7	5.86	138.5	5.64	167.6	6.13
ScII	6245.62	1.51	-1.05	71.6	2.72	92.7	2.72	104.7	2.95	93.4	2.83	88.9	2.75
ScII	6279.74	1.50	-1.16	85.8	3.18	97.6	2.93	115.5	3.26	81.3	2.75	78.1	2.69
ScII	6604.60	1.36	-1.15	91.6	3.03	115.3	2.94	108.5	2.86	92.1	2.68	103.0	2.88
TiI	5866.46	1.07	-0.84	150.8	4.78	210.1	4.94	221.4	5.14	163.7	4.54	196.5	5.01
TiI	5922.12	1.05	-1.47	128.8	4.88	170.0	4.81	185.9	5.16	142.0	4.66	165.9	5.02
TiI	5978.55	1.87	-0.50	111.7	4.77	137.1	4.54	148.6	4.81	122.7	4.58	133.7	4.74
TiI	6091.18	2.27	-0.42			103.3	4.49	114.8	4.74	103.1	4.72	109.9	4.78
TiI	6126.22	1.07	-1.42	128.6	4.81	181.9	4.92	169.9	4.78	149.5	4.71	149.2	4.62
TiI	6258.11	1.44	-0.36	176.6	4.99	220.7	4.95	223.2	5.04	188.3	4.86	187.4	4.80
TiI	6554.24	1.44	-1.22		151.1	4.91							
TiII	6606.98	2.06	-2.90	41.6	5.14	45.4	5.07	32.8	4.84	29.8	4.77	51.4	5.19
Vi	6002.31	1.22	-1.77	59.2	3.76	63.8	3.64	79.3	3.87	70.9	3.92	58.2	3.56
Vi	6039.73	1.06	-0.65			144.5	3.43	159.8	3.76			138.3	3.60
Vi	6081.45	1.05	-0.58			168.9	3.92	174.6	4.10	146.8	3.85	158.3	3.99
Vi	6090.22	1.08	-0.06	133.0	3.62	193.8	3.83	183.2	3.76	158.5	3.59	172.8	3.79
Vi	6111.65	1.04	-0.71			180.7	3.97	178.9	4.02	163.0	4.04		
Vi	6119.53	1.06	-0.32	130.3	3.77	164.9	3.57	174.2	3.80	146.6	3.58	166.2	3.87
Vi	6135.38	1.05	-0.75	118.6	3.80	149.4	3.54	162.2	3.81	140.0	3.71	147.3	3.76
Vi	6199.19	0.29	-1.28	175.0	4.04	217.7	4.01	224.9	4.19	187.9	3.90		
Vi	6216.36	0.28	-0.81			215.6	3.46	224.9	3.68	197.6	3.55	202.6	3.54
Vi	6251.82	0.29	-1.34			188.5	3.63	210.5	4.09	180.9	3.89		
Vi	6256.90	0.28	-2.01	111.1	3.65	167.3	3.88	176.6	4.10			143.4	3.74
Vi	6274.65	0.27	-1.67	121.4	3.58	168.6	3.54	174.5	3.72			158.1	3.65
Vi	6285.17	0.28	-1.51	135.2	3.76	188.6	3.71	194.5	3.89	167.6	3.76	163.8	3.62
Vi	6292.83	0.29	-1.47	152.5	4.03	194.6	3.79	205.5	4.03	174.3	3.86	180.9	3.93
Vi	6531.43	1.22	-0.84			152.5	3.83			128.4	3.77		

4. Metallicities

4.1. Equivalent Widths

The equivalent widths (EWs) were measured on the spectra using the ROSA code (Gratton 1988; see Table 3 for stars member of NGC 6441, and Table 4 for the field stars) with Gaussian fittings to the measured profiles: these exploit a linear relation between EWs and FWHM of the lines, derived from a subset of lines characterized by cleaner profiles (see Bragaglia et al. 2001 for further details on this procedure). Since the observed stars span a very limited atmospheric parameter range, errors in these EWs may be estimated by comparing EWs measures for individual stars with the EW values for each single line averaged over the whole sample. The values listed in Column 9 of Table 2 as errors on the EWs measurements are the *r.m.s.* of residuals around the best fit line for EWs vs. $\langle \text{EWs} \rangle$ (after eliminating a few outliers). These errors may be slightly overestimated, due to real star-to-star

differences. They are roughly reproduced by the formula $\sigma(\text{EW}) \sim 380/(S/N)$ mÅ. Considering the resolution and sampling of the spectra, the errors in the EWs are about 4 times larger than expectations based on photon noise statistics (Cayrel 1988), showing that errors are dominated by uncertainties in the correct positioning of the continuum level; the observed errors could be justified by errors of about 1% for the best cases and about 2% for the worst ones. Due to the problems in background subtraction in the green-yellow part of the spectra, only lines with wavelength > 5800 Å were used.

4.2. Atmospheric Parameters

We performed a standard line analysis on the equivalent widths measured on our spectra, using model atmospheres extracted by interpolation from the grid by Kurucz (1992; models with the overshooting option switched

Table 3. Continued

El.	Wavel.	E.P.	log gf	4050		4434		4463		4487		2961	
	(Å)	(eV)		EW	log A								
				(mÅ)		(mÅ)		(mÅ)		(mÅ)		(mÅ)	
CrI	6330.10	0.94	-2.87	139.6	5.52	189.0	5.51	173.1	5.34	144.6	5.11	157.5	5.28
MnI	6013.50	3.07	-0.25	139.8	5.18	169.3	5.05	187.1	5.30	158.6	5.07	172.2	5.29
MnI	6016.65	3.07	-0.09	125.3	4.88	156.5	4.78	162.3	4.92	145.9	4.79	162.2	5.09
MnI	6021.80	3.08	0.03	122.2	4.83	165.6	4.91	174.9	5.07	141.9	4.73	163.9	5.11
FeI	5855.09	4.61	-1.48	37.3	7.09			58.7	7.34	44.0	7.08	45.2	7.14
FeI	5856.10	4.29	-1.57	46.3	6.98	72.7	7.23	87.5	7.52	66.3	7.17	77.0	7.46
FeI	5858.78	4.22	-2.19	23.3	6.89			37.9	7.13	38.0	7.15	36.2	7.12
FeI	5859.60	4.55	-0.70	68.6	7.02	88.0	6.98	111.3	7.40	90.8	7.10	95.1	7.30
FeI	5862.37	4.55	-0.50	79.5	7.07	99.8	6.99	122.2	7.39	97.3	7.03	104.2	7.28
FeI	5905.68	4.65	-0.76	55.1	6.89	83.3	7.10	89.4	7.23	72.2	6.95	75.4	7.10
FeI	5927.80	4.65	-1.06	40.4	6.80	72.7	7.21	72.5	7.22	62.4	7.06	64.6	7.17
FeI	5929.68	4.55	-1.24	49.8	7.10	65.0	7.12	71.8	7.25	59.7	7.06	55.8	7.03
FeI	5930.19	4.65	-0.29	74.9	6.92	100.5	6.94	116.3	7.26	86.4	6.76	110.0	7.34
FeI	5934.67	3.93	-1.15	92.0	7.17	107.3	6.90	136.6	7.44	110.0	7.08	117.4	7.32
FeI	5956.71	0.86	-4.60	130.0	7.09	187.6	7.24	186.5	7.29	160.3	7.06	176.5	7.36
FeI	5976.79	3.94	-1.33			90.3	6.79	101.5	7.02	97.4	7.03	101.0	7.20
FeI	5984.83	4.73	-0.39			125.9	7.52						
FeI	6003.02	3.88	-1.08	90.5	7.00	120.7	7.00	124.3	7.10	110.4	6.95	121.3	7.26
FeI	6007.97	4.65	-0.82	56.3	6.96	74.4	6.99	82.9	7.16	81.8	7.18	77.4	7.18
FeI	6008.57	3.88	-0.96	96.7	7.03	119.0	6.86	135.8	7.18	108.9	6.80	129.6	7.29
FeI	6027.06	4.08	-1.23	72.9	6.98	108.0	7.21	111.0	7.29	100.3	7.18	93.9	7.14
FeI	6056.01	4.73	-0.42	65.1	6.88	91.9	7.03	86.6	6.95	90.7	7.08	104.1	7.47
FeI	6079.02	4.65	-0.95									68.8	7.15
FeI	6082.72	2.22	-3.57	86.3	7.02	146.0	7.57	141.8	7.53			131.3	7.57
FeI	6089.57	4.58	-1.28					85.3	7.56				
FeI	6093.65	4.61	-1.32	42.6	7.07			60.3	7.20	58.1	7.19	59.1	7.26
FeI	6094.38	4.65	-1.56	34.3	7.15			33.9	7.00	44.1	7.22		
FeI	6096.67	3.98	-1.77	58.8	7.06	79.1	7.09	72.3	6.99	75.3	7.09	75.2	7.14
FeI	6098.25	4.56	-1.81	38.5	7.38								
FeI	6137.00	2.20	-2.95	125.6	7.28	183.9	7.47	171.7	7.34	158.9	7.32	163.8	7.46
FeI	6151.62	2.18	-3.30	99.1	6.99	156.6	7.38	144.2	7.20	127.8	7.06	138.1	7.32
FeI	6173.34	2.22	-2.88	112.4	6.98	159.7	7.07	156.2	7.06	144.2	7.00	153.9	7.26
FeI	6188.00	3.94	-1.63			85.4	7.00	84.6	7.00	77.9	6.94	78.8	7.01
FeI	6200.32	2.61	-2.44	106.0	6.94			146.4	7.02	132.1	6.90	136.7	7.07
FeI	6213.44	2.22	-2.54	149.4	7.26	169.1	6.88	173.9	7.00	156.5	6.89	165.4	7.09
FeI	6219.29	2.20	-2.43	134.5	6.92	188.3	7.00	188.9	7.07	173.4	7.02	177.4	7.13
FeI	6226.74	3.88	-2.08	46.1	6.89	80.0	7.27	57.6	6.90	70.2	7.16	61.3	7.02
FeI	6232.65	3.65	-1.22	97.7	6.96	133.3	7.00	136.3	7.09	130.3	7.09	121.0	7.03
FeI	6240.65	2.22	-3.23	95.8	6.89	131.9	6.93	144.8	7.20	121.3	6.93	130.8	7.17
FeI	6265.14	2.18	-2.55	147.4	7.19	208.5	7.34	209.2	7.39	181.6	7.22	187.4	7.34
FeI	6270.23	2.86	-2.46			121.3	6.92	121.5	6.96			114.7	7.03
FeI	6297.80	2.22	-2.74	146.7	7.42	191.9	7.39	185.0	7.36	159.4	7.14	180.7	7.50
FeI	6301.51	3.65	-0.72	116.7	6.80	161.0	6.89	158.2	6.88			164.1	7.15
FeI	6311.50	2.83	-3.16	76.0	7.19	115.6	7.44	107.7	7.33			101.3	7.38
FeI	6315.81	4.08	-1.68	46.0	6.76	78.4	7.12	72.2	7.02	61.0	6.86	72.2	7.12
FeI	6322.69	2.59	-2.43	119.2	7.16	154.8	7.04	144.8	6.90	137.3	6.92	145.7	7.16
FeI	6330.85	4.73	-1.22	52.0	7.37			59.0	7.24	49.8	7.08	70.7	7.56
FeI	6335.34	2.20	-2.27			220.2	7.17					193.5	7.10
FeI	6380.75	4.19	-1.37			96.3	7.27	92.7	7.23	80.9	7.07	97.7	7.49
FeI	6392.54	2.28	-3.97	78.3	7.25	107.6	7.30	83.8	6.92			90.3	7.14
FeI	6400.32	3.60	-0.23			263.3	7.28					225.1	7.17
FeI	6411.66	3.65	-0.60	129.7	6.87	172.7	6.92					164.8	7.04
FeI	6421.36	2.28	-2.03			235.4	7.16						
FeI	6481.88	2.28	-2.98	119.3	7.26	168.3	7.34	152.2	7.13	140.4	7.08	158.7	7.47

off). Atmospheric parameters defining these model atmospheres were obtained as follows.

Whenever possible, effective temperatures were derived from de-reddened $V - K$ colors, obtained by combining our V magnitudes with K ones drawn from the 2MASS catalog (Cutri et al. 2003), using the calibration by Alonso et al. (1999). The reddening we adopted is $E(B - V) = 0.49$, which is the average value between various literature determinations. Zinn (1980) and Reed et al. (1988) obtained $E(B - V) = 0.47$ and $E(B - V) = 0.49$ respectively from integrated photometry; Layden et al. (1999) and Pritzl et al. (2001) found $E(B - V) = 0.45 \pm 0.05$ and $E(B - V) = 0.51 \pm 0.02$ mag respectively from the blue edge of the RR Lyrae instability strip. For comparison, the maps by Schlegel et al. (1998) give $E(B - V) = 0.616$, but these are known to overestimate reddening for ob-

jects close to the galactic plane, like NGC 6441. Adopted $E(B - V)$ values were transformed into $E(V - K)$ ones using the formula $E(V - K) = 2.75 E(B - V)$ (Cardelli et al. 1989). Errors in these temperatures are not easy to evaluate. Internal photometric errors in the 2MASS $V - K$ colors are generally small (< 0.04 mag), leading to random errors of < 25 K. However, interstellar reddening is probably variable in the field of NGC 6441 (Layden et al. 1999; Pritzl et al. 2001); four of the observed stars lie in the south-east sector of the cluster, where Layden et al. found a reddening value in the range $0.41 < E(B - V) < 0.54$. Assuming an *r.m.s.* scatter of 0.05 mag in $E(B - V)$ (0.14 mag in $E(V - K)$), the random (star-to-star) uncertainties in the effective temperatures may be as large as ± 80 K. Systematic uncertainties are likely larger, including errors in the Alonso et al. color-temperature cal-

Table 3. Continued

El.	Wavel.	E.P.	log gf	4050		4434		4463		4487		2961	
	(Å)	(eV)		EW	log A								
				(mÅ)		(mÅ)		(mÅ)		(mÅ)		(mÅ)	
Fe I	6498.94	0.96	-4.70			216.4	7.73	185.8	7.37	162.0	7.22	184.3	7.59
Fe I	6518.37	2.83	-2.46	114.0	7.40	151.5	7.34	125.1	6.92	120.9	6.97		
Fe I	6533.94	4.56	-1.29			89.4	7.58	58.1	7.05	49.0	6.90	68.6	7.33
Fe I	6574.25	0.99	-5.00	125.7	7.46	183.6	7.60	150.3	7.12	133.9	7.01	150.7	7.34
Fe I	6581.22	1.49	-4.68			157.5	7.63	145.5	7.48	119.8	7.19	134.4	7.48
Fe I	6593.88	2.43	-2.42	137.6	7.17	186.3	7.21	166.6	6.98	153.2	6.92	175.1	7.30
Fe I	6608.04	2.28	-3.96	73.0	7.07	115.8	7.39	99.8	7.16	87.4	7.05	105.7	7.41
Fe I	6609.12	2.56	-2.69			165.3	7.38	153.5	7.24	142.3	7.19	150.5	7.42
Fe I	6627.56	4.55	-1.50					45.4	7.02	38.1	6.89	61.9	7.39
Fe I	6633.76	4.56	-0.82	74.6	7.28	101.6	7.33	80.1	6.97	82.3	7.05	96.5	7.43
Fe I	6703.58	2.76	-3.01	92.7	7.30	128.1	7.34	108.6	7.04	91.0	6.84	109.6	7.23
Fe I	6713.75	4.80	-1.41	41.3	7.37								
Fe I	6725.36	4.10	-2.21	45.4	7.29			35.5	6.92			49.8	7.22
Fe I	6726.67	4.61	-1.10	43.9	6.86	70.7	7.12	60.4	6.96	54.3	6.87	71.0	7.24
Fe I	6733.15	4.64	-1.44	42.7	7.21			42.4	7.02	35.1	6.88	50.5	7.23
Fe I	6750.16	2.42	-2.62	124.7	7.09	181.9	7.28	161.3	7.03	146.3	6.94	157.9	7.20
Fe I	6786.86	4.19	-1.90	52.7	7.28	68.4	7.30	49.8	6.99			61.1	7.26
Fe II	6247.56	3.89	-2.33	24.0	6.91			19.2	6.50	31.7	6.86	28.7	6.92
Fe II	6432.68	2.89	-3.58	22.1	6.80	48.2	7.35	25.3	6.74	26.3	6.70	42.6	7.29
Fe II	6456.39	3.90	-2.10	33.3	7.07	61.5	7.52	38.2	6.93	34.8	6.75	42.5	7.16
Fe II	6516.08	2.89	-3.38	39.2	7.21			67.2	7.56	42.7	6.95	47.8	7.23
Ni I	5847.01	1.68	-3.44	79.3	5.99	108.3	5.99	131.8	6.49	104.5	6.09	110.4	6.28
Ni I	5996.74	4.24	-1.06	22.7	5.70	34.9	5.90	31.1	5.82	31.4	5.82	41.8	6.09
Ni I	6053.69	4.24	-1.07	31.5	5.97	53.6	6.28	40.5	6.03	46.0	6.14		
Ni I	6086.29	4.27	-0.47	46.2	5.82	61.6	5.87	47.5	5.61	47.6	5.61	68.0	6.10
Ni I	6108.12	1.68	-2.49	117.7	5.92	174.9	6.12	157.1	5.90	147.9	5.90	156.2	6.11
Ni I	6111.08	4.09	-0.83	55.4	6.17	72.4	6.17	53.6	5.84	61.5	6.00	63.5	6.10
Ni I	6128.98	1.68	-3.39	76.7	5.80	116.0	6.02	110.6	5.96	101.8	5.93	111.2	6.15
Ni I	6130.14	4.27	-0.98	30.4	5.90	49.1	6.15	38.0	5.93	39.4	5.96	50.1	6.23
Ni I	6176.82	4.09	-0.26	77.0	6.14	81.3	5.76	87.3	5.88	88.3	5.95	83.8	5.96
Ni I	6177.25	1.83	-3.60	63.4	5.90	88.4	5.98	89.7	6.02	90.6	6.14	82.7	5.99
Ni I	6186.72	4.11	-0.90	50.4	6.14	74.2	6.30	46.7	5.80	65.6	6.17	60.0	6.13
Ni I	6204.61	4.09	-1.15	45.2	6.22	66.3	6.38	54.8	6.18	50.8	6.11	61.5	6.38
Ni I	6223.99	4.11	-0.97	46.0	6.09	49.6	5.93	39.8	5.74	53.1	6.00	37.9	5.73
Ni I	6230.10	4.11	-1.20	43.5	6.26	57.9	6.31	53.3	6.23	56.0	6.29	51.0	6.24
Ni I	6322.17	4.15	-1.21			45.4	6.14	20.6	5.59	30.5	5.83	43.3	6.14
Ni I	6327.60	1.68	-3.09							128.0	6.09	138.8	6.35
Ni I	6378.26	4.15	-0.82	49.4	6.08	73.9	6.27	51.4	5.86	50.3	5.85	70.3	6.32
Ni I	6384.67	4.15	-1.00	46.1	6.17	69.4	6.36	44.8	5.92	36.2	5.75	61.1	6.30
Ni I	6482.81	1.93	-2.85	93.0	5.86	148.4	6.24	136.9	6.11	122.4	6.00	126.1	6.10
Ni I	6532.88	1.93	-3.42							95.0	6.14	94.2	6.14
Ni I	6586.32	1.95	-2.79	99.6	6.12	142.1	6.21	125.1	5.96	108.3	5.78	126.0	6.17
Ni I	6598.61	4.24	-0.93			59.0	6.23	36.3	5.80	42.8	5.93	55.1	6.23
Ni I	6635.14	4.42	-0.75	46.3	6.30	57.9	6.28	34.4	5.82	27.1	5.64	52.2	6.24
Ni I	6767.78	1.83	-2.11	131.8	5.87	189.5	6.01	165.8	5.74	148.9	5.61	173.1	6.05
Ni I	6772.32	3.66	-1.01	71.3	6.09	94.8	6.09	74.6	5.76	64.6	5.62	92.7	6.22
Y I	6435.02	0.07	-0.82	54.0	1.05	98.9	1.50	112.1	1.77	62.6	1.23	90.2	1.47
Zr I	6127.46	0.15	-1.06	86.5	2.15	121.9	2.08	116.3	2.05	96.8	1.97	84.9	1.58
Zr I	6134.57	0.00	-1.28	67.2	1.59	99.4	1.70	104.3	1.84	91.8	1.87	87.6	1.62
Zr I	6140.46	0.52	-1.41	36.8	1.57	45.1	1.85	41.5	1.83	26.8	1.73	29.7	1.54
Zr I	6143.18	0.07	-1.10	81.6	1.94	121.0	1.98	106.6	1.80	93.5	1.83	81.8	1.44
Zr I	6445.72	1.00	-0.83			21.9	1.56	18.3	1.49	12.1	1.43	15.4	1.31
Ba II	5853.69	0.60	-1.00	111.5	2.09	148.4	1.84	162.9	2.18	125.2	1.69	140.5	2.09
Ba II	6141.75	0.70	0.00	159.2	1.89	220.6	1.93	205.8	1.82	180.3	1.68	182.9	1.74
Ba II	6496.91	0.60	-0.38	182.2	2.32	221.6	2.14	205.3	1.99	177.4	1.83	196.3	2.10
Eu II	6437.64	1.32	-0.28			34.0	0.65	22.5	0.40	25.1	0.50	24.6	0.42
Eu II	6645.11	1.38	0.20	39.3	0.55	54.6	0.61	48.6	0.52	31.0	0.23	41.0	0.38

ibration, in the photometric calibration, and on the average reddenings we assumed. Hereinafter we will assume possible systematic errors of ± 100 K.

For stars lacking the 2MASS photometry, we used our $V - I$ colors. Since these colors lack a proper photometric calibration, we may use those stars having known $V - K$ colors to construct a correlation between the two colors, that turned out to be very narrow (this is not unexpected, since both colors have a weak dependence on metal abundance). The mean relation is $V - K = 0.479 + 1.952(V - I)$, derived from more than 250 stars spanning over 4 magnitudes in $V - K$ color; the *r.m.s.* scatter around this mean relation is 0.098 mag in $(V - K)$. We could derive consistent temperatures also for stars with only $V - I$ colors,

the errors due to uncertainties in the colors being smaller than those related to the assumptions about reddening.

We may compare these temperatures derived from colors with those that we could deduce from excitation equilibrium for Fe I lines. We found that on average temperatures derived from Fe I excitation equilibrium are lower by 70 ± 27 K, with an *r.m.s.* scatter for individual stars of 95 K. This small difference can be attributed to several causes (errors in the adopted temperature scale, inadequacies of the adopted model atmospheres, etc.). On the whole we do not consider this difference as important. The star-to-star scatter in the difference between temperatures from colors and excitation equilibrium is not much larger than the internal errors in the excitation temperatures

Table 4. Equivalent Widths from UVES spectra for non members (in electronic form)

El.	Wavel. (Å)	E.P. (eV)	log gf	3734 EW (mÅ)	log A	4360 EW (mÅ)	log A	5308 EW (mÅ)	log A	5341 EW (mÅ)	log A	4329 EW (mÅ)	log A	4453 EW (mÅ)	log A	3092 EW (mÅ)	log A
Oi	6300.31	0.00	-9.75	86.2	8.83	63.7	8.82	83.6	8.98	77.0	8.89			69.2	8.78	95.7	8.89
Oi	6363.79	0.02	-10.25	44.0	8.82	39.2	9.03	29.7	8.77					39.3	8.92	50.0	8.78
Nai	6154.23	2.10	-1.57	91.1	6.19	166.3	7.22	100.9	6.42	125.3	6.70	108.9	6.62	113.2	6.50	91.9	6.26
Nai	6160.75	2.10	-1.26	98.9	6.00	169.6	6.96	95.5	6.03	136.0	6.55	129.6	6.63	120.4	6.30	129.6	6.60
Mgi	6318.71	5.11	-1.94	81.4	7.64	132.4	8.40	80.8	7.63	94.4	7.88	89.7	7.82	74.2	7.48	72.1	7.63
Mgi	6319.24	5.11	-2.16	57.6	7.44	102.6	8.16	39.2	7.14	70.4	7.71	80.9	7.88	61.1	7.49	64.2	7.69
AlI	6696.03	3.14	-1.32	88.7	6.05	144.7	6.88	118.1	6.66	115.0	6.46	103.6	6.46	118.1	6.52	98.2	6.28
AlI	6698.67	3.14	-1.62	59.2	5.87	109.9	6.64	99.3	6.64	77.1	6.14	64.1	6.09	79.3	6.21	69.8	6.02
SiI	5948.55	5.08	-1.23	81.3	7.55	121.7	8.18	62.6	7.13	85.1	7.68	104.5	7.85	93.4	7.67	58.2	7.33
SiI	6125.03	5.62	-1.57			84.3	8.55					48.0	7.76				
SiI	6145.02	5.62	-1.49	45.2	7.77	87.6	8.51	37.5	7.53	25.7	7.38	50.7	7.74	36.0	7.51	28.7	7.55
CaI	5857.46	2.93	0.24	168.3	5.77	213.9	6.25	165.6	5.86	195.1	6.02	201.9	6.32	204.5	6.14	128.0	5.34
CaI	5867.57	2.93	-1.49	58.8	5.65	97.1	6.30	70.3	6.01	105.2	6.49	83.3	6.31	79.1	6.04	80.0	6.12
CaI	6161.30	2.52	-1.27	129.5	6.16	160.8	6.56	120.8	6.16	147.7	6.40			142.2	6.32	110.3	5.93
CaI	6166.44	2.52	-1.14	121.0	5.88	163.0	6.47	124.7	6.10								
CaI	6169.04	2.52	-0.80	159.5	6.14	192.2	6.52			166.6	6.20	162.4	6.44	158.7	6.12	121.5	5.68
CaI	6169.56	2.52	-0.48	159.4	5.82	196.9	6.25			195.4	6.20	179.2	6.32	167.5	5.92	149.2	5.74
CaI	6439.08	2.52	0.39	211.3	5.64	243.6	5.93	211.9	5.78	223.3	5.72	222.4	6.00	229.5	5.82	185.4	5.41
CaI	6449.82	2.52	-0.50	171.2	6.10	193.2	6.29	175.1	6.30	196.3	6.35	177.3	6.44	190.8	6.30		
CaI	6455.60	2.52	-1.29	106.4	5.75	141.0	6.24	122.2	6.22	123.4	5.99	118.6	6.21	128.8	6.10	101.4	5.77
CaI	6462.57	2.52	0.26	271.5	6.16	315.6	6.50	272.3	6.31	274.2	6.20	262.9	6.39	281.3	6.30	226.1	5.84
CaI	6471.67	2.52	-0.69	148.0	5.94	185.6	6.38	156.0	6.22			155.6	6.30	157.2	6.02	125.8	5.71
CaI	6493.79	2.52	-0.11	185.7	5.90	217.3	6.19	188.0	6.06	186.6	5.86	177.3	6.05	191.6	5.93	154.3	5.57
CaI	6499.65	2.52	-0.82	145.2	6.02	177.6	6.39	141.7	6.11	151.9	6.06	147.0	6.28				
ScII	6245.62	1.51	-1.05			99.5	3.24	91.3	3.15	105.6	3.44	89.9	3.21	87.9	2.96	56.1	2.45
ScII	6279.74	1.50	-1.16	72.6	2.80	82.0	3.06	97.2	3.41	109.9	3.65	71.5	2.98	85.1	3.04	59.5	2.66
ScII	6604.60	1.36	-1.15	94.5	2.98	133.5	3.70			76.6	2.74	71.8	2.73	116.6	3.36	84.0	2.96
TiI	5866.46	1.07	-0.84	162.8	4.86	200.9	5.40	164.7	5.14	183.9	5.16	165.9	5.31	186.7	5.25		
TiI	5922.12	1.05	-1.47	143.5	5.03			141.3	5.25	162.8	5.30	137.1	5.30	148.1	5.06	110.1	4.42
TiI	5978.55	1.87	-0.50	114.8	4.72	144.0	5.14	127.1	5.20	147.9	5.29	124.3	5.24	130.4	4.97	95.3	4.36
TiI	6091.18	2.27	-0.42	111.4	5.16	132.3	5.42	94.4	4.96	119.1	5.24	90.2	4.95	104.9	4.96	96.4	4.93
TiI	6126.22	1.07	-1.42	147.0	5.02	159.8	5.11	145.5	5.24	160.0	5.17	122.2	4.90	157.8	5.15	129.0	4.84
TiI	6258.11	1.44	-0.36	159.9	4.71	190.3	5.12	159.8	4.94	198.4	5.24			172.6	4.89	128.5	4.32
TiI	6554.24	1.44	-1.22	114.6	4.62	155.8	5.26	112.5	4.82			127.5	5.21	138.2	5.02		
TiII	6606.98	2.06	-2.90	24.5	4.75	66.0	5.72	28.6	4.92	36.5	5.19	38.1	5.21	63.7	5.60	30.4	4.95
VI	6002.31	1.22	-1.77	38.7	3.51	89.0	4.39	52.1	3.98	72.3	4.08	45.6	3.96	56.6	3.94	71.4	4.03
VI	6039.73	1.06	-0.65	110.9	3.46	159.9	4.26	109.1	3.67	140.2	3.99	117.0	3.96	132.6	3.85	117.3	3.79
VI	6081.45	1.05	-0.58	126.1	3.80	163.2	4.38			159.7	4.36	130.6	4.26	157.4	4.32	128.9	4.03
VI	6090.22	1.08	-0.06	148.7	3.76	183.2	4.27	138.8	3.83	177.6	4.19	138.8	3.97	167.2	4.04	147.9	3.87
VI	6111.65	1.04	-0.71			135.9	4.20	174.0	4.54	174.0	4.54	136.8	4.35	147.7	4.08		
VI	6119.53	1.06	-0.32	134.1	3.71	185.3	4.50	128.1	3.83	162.8	4.16	125.4	3.90	147.0	3.88	131.3	3.82
VI	6135.38	1.05	-0.75	119.8	3.70	166.4	4.39	118.3	3.91	145.9	4.09	116.9	3.98	135.2	3.92	108.0	3.56
VI	6199.19	0.29	-1.28	170.3	3.94	202.1	4.42	172.6	4.26	211.8	4.56	171.7	4.39	202.6	4.48	159.5	3.85
VI	6216.36	0.28	-0.81	179.7	3.58	211.2	4.04	172.3	3.74	215.9	4.09	171.6	3.88	198.1	3.88		
VI	6242.81	0.26	-1.55			174.1	4.15	138.7	3.94								
VI	6251.82	0.29	-1.34			158.7	4.14	190.8	4.38	147.0	4.07	147.0	4.07	188.2	4.37	129.1	3.40
VI	6256.90	0.28	-2.01	125.6	3.90	166.3	4.50	112.5	3.91	145.6	4.18	114.8	4.06	137.9	4.08	120.0	3.93
VI	6274.65	0.27	-1.67			132.2	3.97	163.0	4.14	125.1	3.94	153.5	3.99	118.5	3.99	118.5	3.54
VI	6285.17	0.28	-1.51			134.4	3.86	175.8	4.25	146.9	4.22	166.0	4.08	136.8	3.83		
VI	6292.83	0.29	-1.47			155.4	4.21	207.2	4.66	137.8	4.03						
VI	6531.43	1.22	-0.84	97.3	3.48	169.1	4.62	107.0	3.91	127.9	4.02			122.9	3.94	105.5	3.77

alone (68 K). This leaves space for errors in temperatures from colors of about 66 K, to be attributed to the effect of differential reddening. This corresponds to an r.m.s scatter of about 0.043 mag in the reddening, compatible with results from photometry alone.

Surface gravities were obtained from the location of the stars in the color-magnitude diagram. This procedure requires assumptions about the distance modulus; (we adopted $(m - M)_V = 16.33$ from Harris (1996) for the cluster members, while for the field bulge stars we assumed that the stars are at the same distance of the galactic center: 7.9 ± 0.3 kpc from Eisenhauer et al. (2003), the bolometric corrections (from Alonso et al. 1999), and the masses (we assumed a mass of $0.9 M_\odot$, close to the value given by isochrone fittings). Uncertainties in these gravities are small for cluster stars (we estimate internal star-to-star errors of about 0.06 dex, due to the effects of possible variations in the interstellar absorption; and sys-

tematic errors of about 0.15 dex, dominated by systematic effects in the temperature scale).

We may compare these values for the surface gravities with those deduced from the equilibrium of ionization of Fe. On average, abundances from Fe II lines are 0.01 ± 0.05 dex smaller than that derived from Fe I lines. The agreement is obviously very good. The star-to-star scatter in the residuals is 0.17 dex, but it is as small as 0.12 dex if only stars member of NGC 6441 are considered; this last value is close to the value expected considering that only three to four Fe II lines were typically used in the analysis. The larger spread obtained for field stars is not unexpected, since these stars may be at different distances from the Sun.

Micro-turbulence velocities v_t were determined by eliminating trends in the relation between expected line strength and abundances (see Magain 1984). The error on the micro-turbulent velocities is determined by the

Table 4. Continued

El.	Wavel.	E.P.	log gf	3734		4360		5308		5341		4329		4453		3092	
	(Å)	(eV)		EW	log A												
				(mÅ)		(mÅ)		(mÅ)		(mÅ)		(mÅ)		(mÅ)		(mÅ)	
CrI	6330.10	0.94	-2.87	121.9	5.04	180.7	5.98	131.6	5.46	155.2	5.60			149.4	5.48	150.2	5.72
MnI	6013.50	3.07	-0.25	144.8	5.14	203.3	5.84	139.8	5.16	182.6	5.61	183.0	5.81	178.5	5.53	121.1	4.98
MnI	6016.65	3.07	-0.09	155.2	5.18	192.8	5.66	141.4	5.10	172.4	5.43	168.0	5.58	160.1	5.23	113.6	4.72
MnI	6021.80	3.08	0.03	138.3	4.96	215.1	5.85	136.4	5.02	174.3	5.44	166.6	5.55	171.0	5.36	121.9	4.89
FeI	5835.11	4.26	-2.18	35.5	7.23	76.3	8.30							63.2	7.80		
FeI	5855.09	4.61	-1.48	43.7	7.19			49.8	7.35	49.0	7.36	60.8	7.64	54.9	7.40	37.4	7.17
FeI	5856.10	4.29	-1.57	69.1	7.42	95.5	7.90	60.3	7.25	88.6	7.89	81.1	7.80	81.7	7.60		
FeI	5858.78	4.22	-2.19	29.7	7.05			33.5	7.50	42.5	7.42	46.3	7.52	42.7	7.36		
FeI	5859.60	4.55	-0.70	84.0	7.20			81.6	7.16	114.2	7.80	115.7	7.94	111.4	7.63	73.6	7.25
FeI	5862.37	4.55	-0.50	99.1	7.31	116.3	7.54	81.3	6.95	110.4	7.54	124.4	7.88	104.0	7.30	84.3	7.28
FeI	5881.28	4.61	-1.76	39.3	7.36			47.8	7.58	68.4	8.04			59.6	7.76		
FeI	5902.48	4.59	-1.86					49.9	7.71	41.1	7.55	53.7	7.84	43.3	7.52		
FeI	5905.68	4.65	-0.76	81.7	7.38	124.1	8.10	81.3	7.37								
FeI	5927.80	4.65	-1.06	63.4	7.26	87.3	7.69	58.0	7.15	81.0	7.67	78.4	7.66	65.1	7.22	49.1	7.14
FeI	5929.68	4.55	-1.24	73.5	7.53	100.5	8.00	51.0	7.05	86.4	7.83	79.6	7.74	73.8	7.44	49.0	7.17
FeI	5930.19	4.65	-0.29			150.8	8.06	91.0	7.11	125.9	7.77	125.9	7.88	118.9	7.52	92.2	7.45
FeI	5934.67	3.93	-1.15	98.1	7.12	131.1	7.65	123.5	7.65	145.4	7.96	134.5	7.94	129.3	7.59	101.9	7.50
FeI	5956.71	0.86	-4.60	159.0	7.41			147.5	7.41	163.0	7.52	143.9	7.51	129.3	7.58		
FeI	5976.79	3.94	-1.33	88.1	7.10			84.9	7.07	119.7	7.76	114.7	7.82	111.6	7.48	68.5	6.92
FeI	5984.83	4.73	-0.39	103.6	7.48			89.5	7.22	135.1	7.98					99.2	7.65
FeI	6003.02	3.88	-1.08	110.3	7.24	142.9	7.72	107.3	7.22	135.2	7.68	134.9	7.82	127.7	7.44	107.9	7.47
FeI	6007.97	4.65	-0.82	67.8	7.09	101.9	7.70	73.9	7.24	81.0	7.40	97.6	7.82	84.4	7.35		
FeI	6008.57	3.88	-0.96	109.9	7.12	146.9	7.68	102.8	7.02	129.6	7.48	134.2	7.70	130.5	7.38	88.6	6.97
FeI	6027.06	4.08	-1.23	104.6	7.55	118.0	7.69	97.7	7.44	114.9	7.76	101.9	7.62	102.7	7.39	88.2	7.50
FeI	6056.01	4.73	-0.42	86.8	7.25	111.2	7.62	88.0	7.28	102.6	7.58	104.2	7.71	92.7	7.25		
FeI	6078.50	4.80	-0.48			127.8	7.99	100.5	7.60	110.9	7.80	108.6	7.85	99.9	7.49	71.0	7.28
FeI	6079.02	4.65	-0.95	76.9	7.45	104.6	7.92	66.5	7.23	89.0	7.73			79.1	7.40	68.5	7.55
FeI	6082.72	2.22	-3.57	112.7	7.50			119.4	7.77	135.0	7.96	116.1	7.82	123.3	7.60		
FeI	6089.57	4.58	-1.28					94.0	8.03	85.6	7.93	93.8	7.90				
FeI	6093.65	4.61	-1.32	64.5	7.49			60.6	7.42	59.0	7.40	61.4	7.49	61.5	7.36	58.2	7.59
FeI	6094.38	4.65	-1.56	43.4	7.31			40.2	7.27	41.1	7.32	48.0	7.48	45.2	7.34		
FeI	6096.67	3.98	-1.77	73.2	7.26	109.2	7.93	78.1	7.41	86.0	7.56	85.1	7.64	79.0	7.30	54.1	7.02
FeI	6098.25	4.56	-1.81	47.1	7.52			46.4	7.54	58.5	7.82	55.3	7.78	55.9	7.68		
FeI	6137.00	2.20	-2.95	135.3	7.26	157.4	7.56	146.0	7.56	164.4	7.77	147.8	7.73	170.5	7.77		
FeI	6151.62	2.18	-3.30	135.2	7.59	148.8	7.72	118.7	7.38	123.3	7.34	121.7	7.56	137.1	7.50	103.0	7.21
FeI	6165.36	4.14	-1.50	70.1	7.19	96.8	7.60	63.1	7.02	88.7	7.56	84.5	7.55	77.0	7.20	50.9	6.89
FeI	6173.34	2.22	-2.88	147.7	7.44	184.9	7.94			165.7	7.74	144.0	7.62	154.8	7.47	126.0	7.35
FeI	6188.00	3.94	-1.63	81.0	7.22			76.9	7.18	97.6	7.59	97.8	7.73	81.2	7.15	59.2	6.96
FeI	6200.32	2.61	-2.44	151.2	7.59	160.4	7.66	121.6	7.18	159.4	7.74	138.9	7.62	149.2	7.47		
FeI	6226.74	3.88	-2.08	73.2	7.42	79.1	7.50	59.1	7.17	66.0	7.30	72.0	7.51	61.0	7.13	57.0	7.26
FeI	6232.65	3.65	-1.22	140.0	7.52	179.2	8.03	123.7	7.34	141.8	7.59	131.6	7.58	135.4	7.38		
FeI	6240.65	2.22	-3.23	128.9	7.45	148.5	7.69	108.1	7.14	121.5	7.29			133.3	7.42	101.3	7.15
FeI	6246.33	3.60	-0.73	140.4	6.98			136.2	6.97								
FeI	6265.14	2.18	-2.55	169.2	7.35			168.6	7.47							147.5	7.27
FeI	6270.23	2.86	-2.46			137.1	7.60	104.8	7.19	129.8	7.60	125.4	7.74	122.7	7.34	90.9	7.07
FeI	6297.80	2.22	-2.74					155.0	7.52	168.2	7.64	148.6	7.55	170.8	7.59	128.7	7.26
FeI	6301.51	3.65	-0.72	142.6	7.04			162.7	7.32	152.3	7.20	160.1	7.44				
FeI	6311.50	2.83	-3.16	101.5	7.65	121.2	7.92	96.7	7.62	116.2	7.94	95.3	7.68	108.4	7.67	93.2	7.76
FeI	6315.81	4.08	-1.68	78.0	7.39	91.8	7.59	77.5	7.41	90.9	7.68	70.4	7.32	82.6	7.40	78.1	7.67
FeI	6322.69	2.59	-2.43	140.6	7.34	175.0	7.80	148.4	7.56	151.2	7.53	147.3	7.68	156.3	7.50	120.5	7.28
FeI	6330.85	4.73	-1.22	49.2	7.20			61.4	7.47	71.1	7.70	70.6	7.73	48.3	7.15		
FeI	6380.75	4.19	-1.37	80.0	7.28			96.6	7.65	103.2	7.77	101.8	7.85	102.1	7.62	76.8	7.48
FeI	6392.54	2.28	-3.97	79.6	7.16	111.8	7.76	83.4	7.36	84.4	7.30	82.7	7.44	95.3	7.44	77.7	7.34
FeI	6411.66	3.65	-0.60	143.2	6.92			155.4	7.12					167.8	7.18		
FeI	6481.88	2.28	-2.98	136.0	7.36	179.4	7.99	150.3	7.71	152.5	7.67	137.5	7.64	160.1	7.68	125.3	7.47
FeI	6498.94	0.96	-4.70	147.3	7.35	198.5	8.10	160.0	7.74	174.3	7.83			184.5	7.89	139.2	7.47

change required on the derived v_t to vary the expected line strength vs abundances slope by 1σ . This implies an expected random error in the micro-turbulence velocities of $\pm 0.12 \text{ km s}^{-1}$.

Finally, the model atmospheres were iteratively chosen with model metal abundances in agreement with derived Fe abundance. The adopted model atmosphere parameters are listed in Table 5.

4.3. Fe Abundances

Individual $[\text{Fe}/\text{H}]$ values are listed in Table 6, as well as averages over the whole sample. Reference solar abundances are as in Gratton et al. (2003). Throughout our analysis, we use the same line parameters discussed in

Gratton et al. (2003); in particular, collisional damping was considered using updated constants from Barklem et al. (2000). We note that, for internal consistency, we used four FeII lines for all member stars. In the case of star # 7004463 the lines yield considerably different FeII abundances, therefore the derived *r.m.s.* is larger than in other cases.

Table 7 lists the impact of various uncertainties on the derived abundances for the elements considered in our analysis. Variations in parameters of the model atmospheres were obtained by changing each of the parameters at a time for the star #7004487, assumed to be representative of all the stars considered in this paper. The first three rows of the Table give the variation of the parameter used to estimate sensitivities, the internal (star-to-star) errors

Table 4. Continued

El.	Wavel.	E.P.	log gf	3734	4360	5308	5341	4329	4453	3092	log A	EW	log A	EW	log A	EW	log A
	(Å)	(eV)		EW		(mÅ)		(mÅ)		(mÅ)							
				log A													
FeI	6518.37	2.83	-2.46	108.5	7.06	140.6	7.54										
FeI	6533.94	4.56	-1.29	59.2	7.24	92.1	7.84										
FeI	6574.25	0.99	-5.00	125.2	7.23	165.7	7.89	122.7	7.35	136.4	7.46	121.8	7.46	147.8	7.58	109.9	7.20
FeI	6581.22	1.49	-4.68			123.0	7.52	129.4	7.87	125.5	7.67	116.3	7.74	139.9	7.83	111.0	7.66
FeI	6593.88	2.43	-2.42	144.2	7.11			160.5	7.47	155.8	7.33	158.4	7.58	175.3	7.50	133.0	7.20
FeI	6608.04	2.28	-3.96	82.0	7.18	131.2	8.08	94.6	7.56	97.3	7.53	96.1	7.69	92.2	7.35	83.6	7.45
FeI	6609.12	2.56	-2.69	130.9	7.34	174.5	7.95	134.6	7.50	149.3	7.68	141.6	7.75	164.7	7.80	108.0	7.21
FeI	6627.56	4.55	-1.50	40.2	7.03			55.4	7.38	55.7	7.42	59.5	7.52	82.7	7.85	35.4	7.04
FeI	6633.76	4.56	-0.82	83.2	7.30	119.5	7.88	100.0	7.65	88.8	7.43	109.4	7.92	107.6	7.66	77.3	7.48
FeI	6703.58	2.76	-3.01	87.7	7.02	129.3	7.75	101.6	7.42	102.1	7.34	100.8	7.49	119.4	7.57	83.6	7.20
FeI	6713.75	4.80	-1.41	42.5	7.33			45.9	7.41	30.8	7.13	38.1	7.28	56.2	7.57		
FeI	6725.36	4.10	-2.21			70.1	7.72	50.0	7.37	40.4	7.20	60.7	7.64	64.0	7.58	34.4	7.08
FeI	6726.67	4.61	-1.10	57.2	7.07	82.4	7.52	69.7	7.34			77.2	7.55	75.7	7.37	37.8	6.78
FeI	6733.15	4.64	-1.44	32.4	6.91	79.3	7.85	54.1	7.40	61.2	7.59	54.6	7.46	80.2	7.86	53.6	7.60
FeI	6750.16	2.42	-2.62	136.3	7.11	167.2	7.53	160.8	7.61	157.2	7.49	150.9	7.59	169.0	7.56	123.2	7.18
FeI	6786.86	4.19	-1.90	41.9	6.97	85.2	7.80	61.8	7.42	49.3	7.19	61.9	7.47	78.4	7.66	48.7	7.28
FeII	5991.38	3.15	-3.56	31.0	7.31			46.0	7.67					37.0	7.42		
FeII	6084.10	3.20	-3.80							30.2	7.75	35.0	7.70	35.2	7.67		
FeII	6113.33	3.22	-4.13					27.1	7.78			23.8	7.70				
FeII	6149.25	3.89	-2.73					49.1	7.86	21.1	7.22	27.1	7.21	29.2	7.27		
FeII	6247.56	3.89	-2.33			52.5	7.64	54.3	7.60	54.3	7.87	43.2	7.33	41.5	7.24	27.6	7.27
FeII	6369.46	2.89	-4.21	25.5	7.47	28.0	7.64	32.1	7.62			28.7	7.55	27.1	7.48		
FeII	6416.93	3.89	-2.70	33.4	7.49					29.1	7.50						
FeII	6432.68	2.89	-3.58	35.3	7.15	65.4	7.93	56.4	7.64	30.6	7.18	38.9	7.22	45.0	7.34	24.1	7.07
FeII	6456.39	3.90	-2.10	39.5	7.10	75.6	7.97	58.3	7.50	47.6	7.48	44.7	7.16	55.6	7.40	21.8	6.82
FeII	6516.08	2.89	-3.38	53.5	7.45			63.9	7.62								
NiI	5847.01	1.68	-3.44	102.3	6.39	132.0	6.92	104.1	6.55	113.0	6.67					90.3	6.39
NiI	5996.74	4.24	-1.06	38.9	6.10	67.6	6.72	39.1	6.12	42.6	6.27	54.0	6.51	47.8	6.28	45.0	6.44
NiI	6053.69	4.24	-1.07	37.5	6.08	84.3	7.06	28.8	5.88	64.7	6.76	55.7	6.56	48.9	6.31		
NiI	6086.29	4.27	-0.47	52.5	5.87	98.2	6.78	65.2	6.16	88.0	6.70	77.5	6.50	73.0	6.24	55.2	6.18
NiI	6108.12	1.68	-2.49	139.7	6.13	178.3	6.70	134.8	6.17	154.1	6.41	136.9	6.34	162.0	6.43	124.7	6.17
NiI	6111.08	4.09	-0.83	65.4	6.28	95.4	6.82	66.2	6.30	65.1	6.31	73.1	6.52	71.1	6.32	49.1	6.11
NiI	6128.98	1.68	-3.39	107.8	6.41	132.7	6.80	89.7	6.10	108.0	6.42	107.6	6.63	110.8	6.37	81.0	6.02
NiI	6130.14	4.27	-0.98	32.7	5.92	77.0	6.86	34.3	5.97	46.6	6.31	47.0	6.31	52.4	6.33	37.8	6.20
NiI	6176.82	4.09	-0.26	91.9	6.29	110.0	6.53	87.8	6.22	93.6	6.34	93.2	6.41	91.9	6.17	51.1	5.60
NiI	6177.25	1.83	-3.60	80.0	6.19	102.3	6.63	78.9	6.28	104.3	6.76	77.8	6.35	77.1	6.12		
NiI	6186.72	4.11	-0.90	43.0	5.87	89.7	6.81	59.4	6.25	78.0	6.69	70.6	6.55	57.7	6.14		
NiI	6204.61	4.09	-1.15	61.4	6.51	99.9	7.23	58.7	6.46	37.4	6.04	64.5	6.64	65.7	6.53		
NiI	6223.99	4.11	-0.97	49.9	6.09	75.0	6.60	52.2	6.16	67.6	6.53	58.8	6.36	47.0	6.00	28.0	5.68
NiI	6230.10	4.11	-1.20	47.1	6.26	83.9	7.00	53.6	6.42	69.0	6.79	52.6	6.45	52.3	6.34	31.7	6.02
NiI	6322.17	4.15	-1.21	34.8	6.03	75.6	6.88	33.8	6.03	25.5	5.89	48.3	6.40	30.9	5.95		
NiI	6327.60	1.68	-3.09	117.8	6.28			121.4	6.47	132.8	6.57	124.1	6.65	142.5	6.64	101.0	6.20
NiI	6378.26	4.15	-0.82	51.5	6.02	107.7	7.11	77.0	6.60	57.6	6.22	66.7	6.43	65.8	6.27	54.1	6.32
NiI	6384.67	4.15	-1.00	38.6	5.91	85.5	6.86	66.5	6.54	56.7	6.38	58.4	6.42	70.4	6.54	39.5	6.10
NiI	6482.81	1.93	-2.85	110.0	6.08	149.3	6.72	128.4	6.47	129.1	6.45	106.9	6.27	132.4	6.41	103.4	6.14
NiI	6532.88	1.93	-3.42	81.0	6.12	117.8	6.81	93.5	6.50	106.5	6.71	93.1	6.60	94.2	6.36	66.4	5.98
NiI	6586.32	1.95	-2.79	108.3	6.12	158.6	6.96			122.7	6.42	114.9	6.48	133.3	6.50	92.3	6.05
NiI	6598.61	4.24	-0.93	31.1	5.78	81.8	6.83	59.7	6.43	48.6	6.26	50.5	6.28	67.1	6.52	52.1	6.50
NiI	6635.14	4.42	-0.75	32.6	5.88	80.0	6.86	51.6	6.32	34.2	6.00	51.5	6.36	46.5	6.17	29.1	5.92
NiI	6767.78	1.83	-2.11	145.3	5.92	182.6	6.41	157.4	6.22	152.4	6.07	146.0	6.17	168.9	6.20	124.4	5.86
NiI	6772.32	3.66	-1.01	68.9	5.89	103.1	6.51	79.4	6.15	78.0	6.14	84.5	6.32	87.3	6.19	63.9	6.04
YI	6435.02	0.07	-0.82	61.7	1.30	126.3	2.54	50.1	1.41	75.7	1.57	56.4	1.62	84.0	1.82	64.2	1.27
ZrI	6127.46	0.15	-1.06	85.2	2.00	118.9	2.64	78.8	2.18	89.6	2.07	72.4	2.16	86.7	2.10	79.6	2.02
ZrI	6134.57	0.00	-1.28	87.0	2.03	96.2	2.21	73.7	2.07	78.0	1.84	60.3	1.91	78.0	1.94	85.7	2.16
ZrI	6140.46	0.52	-1.41	26.7	1.75					25.1	1.79	39.0	2.40	42.7	2.26	38.2	1.75
ZrI	6143.18	0.07	-1.10	74.7	1.69	116.3	2.51	73.0	1.98	98.7	2.17	72.7	2.09	87.9	2.04	98.8	2.40
ZrI	6445.72	1.00	-0.83	14.0	1.50	26.9	2.07										
BaII	5853.69	0.60	-1.00	128.3	2.28	121.3	1.94	124.3	2.35	122.9	2.16	132.4	2.69	147.2	2.47	102.3	2.10
BaII	6141.75	0.70	0.00	185.0	2.08	212.4	2.44	170.5	2.07	197.6	2.30	172.1	2.26	190.1	2.14	150.7	1.86
BaII	6496.91	0.60	-0.38			194.3	2.44	166.5	2.24	183.0	2.36	167.1	2.41	173.3	2.10	168.5	2.25
EuII	6437.64	1.32	-0.28			35.7	1.04	33.4	0.94	18.6	0.58	29.9	0.94	28.9	0.80	15.2	0.27
EuII	6645.11	1.38	0.20	28.9	0.30	50.6	0.92	46.0	0.81	39.6	0.69	34.3	0.64	44.5	0.72	31.1	0.40

(for member stars of NGC 6441), and the systematic errors (common to all stars) in each parameter. The first column gives the average number of lines n used for each element. Columns 3-6 give the sensitivities of the abundance ratios to variations of each parameter. Column 7 gives the contribution to the error given by uncertainties in EWs for individual lines: that is $0.194/\sqrt{n}$, where 0.194 is the error in the abundance derived from an individual line, as obtained by the median error over all the stars (note that the errors in the EWs have much smaller impact for the stars having better spectra, like #7004487 itself). The

two final Columns give the total resulting internal and systematic errors, obtained by summing quadratically the contribution of the individual sources of errors, weighted according to the errors appropriate for each parameter. For the systematic errors, the contribution due to equivalent widths and to micro-turbulence velocities (quantities derived from our own analysis), were divided by the square root of the number of cluster members observed. Note that this error analysis does not include the effects of covariances in the various error sources, which are however expected to be quite small for the program stars.

Table 7. Sensitivity of derived abundances to different sources of error.

Element	Average n. lines	T_{eff}	$\log g$	[A/H]	v_t	EWs	Total Internal	Total Systematic
Variation		100	0.30	0.20	0.20			
Internal		50	0.06	0.07	0.12	0.194		
Systematic		100	0.15	0.08	0.12	0.194		
[Fe/H]I	55.0	-0.012	+0.063	+0.028	-0.114	0.026	0.075	0.053
[Fe/H]II	2.7	-0.210	+0.199	+0.046	-0.046	0.119	0.167	0.262
[O/Fe]I	1.8	+0.041	+0.057	+0.009	+0.101	0.145	0.161	0.155
[Na/Fe]I	2.0	+0.106	-0.069	-0.025	+0.039	0.137	0.152	0.177
[Mg/Fe]I	2.0	-0.024	-0.010	-0.013	+0.084	0.137	0.149	0.141
[Al/Fe]I	2.0	+0.087	-0.060	-0.028	+0.062	0.137	0.152	0.166
[Si/Fe]I	2.2	-0.102	+0.020	-0.004	+0.079	0.131	0.151	0.168
[Ca/Fe]I	11.4	+0.131	-0.102	-0.016	-0.006	0.057	0.093	0.152
[Sc/Fe]II	2.8	-0.017	+0.065	+0.008	+0.027	0.115	0.120	0.121
[Ti/Fe]I	6.3	+0.167	-0.050	-0.014	-0.061	0.078	0.123	0.187
[Ti/Fe]II	1.0	-0.048	+0.071	+0.009	+0.095	0.194	0.206	0.205
[V/Fe]I	12.8	+0.178	-0.041	-0.011	-0.077	0.054	0.117	0.188
[Cr/Fe]I	1.0	+0.150	-0.025	-0.015	-0.055	0.194	0.212	0.246
[Mn/Fe]I	3.0	+0.053	-0.063	+0.007	-0.026	0.112	0.120	0.128
[Ni/Fe]I	23.5	-0.028	+0.029	-0.001	+0.032	0.040	0.054	0.052
[Y/Fe]I	1.0	+0.231	-0.044	-0.018	+0.074	0.194	0.230	0.252
[Zr/Fe]I	4.8	+0.207	-0.025	-0.014	+0.043	0.091	0.141	0.213
[Ba/Fe]II	3.0	+0.029	+0.029	+0.014	-0.111	0.112	0.134	0.120
[Eu/Fe]II	1.8	-0.004	+0.058	+0.009	+0.093	0.145	0.156	0.091

Table 5. Atmospheric Parameters for stars observed with UVES

Star	T_{eff} (K)	$\log g$	[A/H]	v_t (km s ⁻¹)
Stars of NGC 6441				
7004050	3956	1.35	-0.40	0.90
7004434	3984	1.40	-0.40	1.75
7004463	4000	1.41	-0.40	1.70
7004487	4074	1.48	-0.40	1.55
8002961	3942	1.23	-0.40	1.40
Field stars				
6003734	4061	1.53	-0.28	1.20
6004360	4163	1.68	0.26	1.55
6005308	4214	1.77	-0.17	1.20
6005341	4079	1.67	0.05	1.35
7004329	4257	1.73	0.11	1.15
7004453	4176	1.69	-0.05	1.45
8003092	3887	1.32	-0.32	0.80

Errors in Fe abundances from neutral lines are dominated by uncertainties in the micro-turbulent velocity. We note that internal errors in Fe I abundances are dominated by errors in v_t . We estimate total random errors of 0.075 dex, and systematic errors of 0.053 dex. From Table 6, the average Fe abundance from all stars of NGC 6441 is $[\text{Fe}/\text{H}] = -0.39 \pm 0.04$ (error of the mean), with an *r.m.s.* scatter of 0.09 dex from 5 stars. The first result of our analysis is that the metallicity of NGC 6441 is $[\text{Fe}/\text{H}] = -0.39 \pm 0.04 \pm 0.05$, where the first error bar includes the uncertainties related to star-to-star random

Table 6. Iron abundances for stars observed with UVES

Star	Fe I		Fe II	
	n	[Fe/H] <i>r.m.s.</i>	n	[Fe/H] <i>r.m.s.</i>
Stars of NGC 6441				
7004050	52	-0.45 0.18	4	-0.49 0.18
7004434	52	-0.34 0.23	2	-0.05 0.12
7004463	57	-0.38 0.18	4	-0.56 0.46
7004487	51	-0.50 0.13	4	-0.68 0.11
8002961	59	-0.28 0.16	4	-0.34 0.16
$\langle [\text{Fe}/\text{H}] \text{I} \rangle = -0.39 \pm 0.04, r.m.s.=0.09$				
$\langle [\text{Fe}/\text{H}] \text{II} \rangle = -0.42 \pm 0.11, r.m.s.=0.24$				
Field stars				
6003734	63	-0.25 0.20	6	-0.16 0.17
6004360	44	+0.27 0.24	7	+0.49 0.27
6005308	63	-0.17 0.21	8	+0.17 0.11
6005341	60	+0.06 0.23	6	+0.01 0.28
7004329	57	+0.12 0.16	7	-0.08 0.24
7004453	62	-0.04 0.20	7	-0.09 0.14
8003092	46	-0.25 0.23	3	-0.44 0.23

errors, and the second one the systematic effects related to the various assumptions made in the analysis. The offset between abundances given by neutral and singly ionized Fe lines is only 0.03 dex, supporting our analysis. The star-to-star scatter (0.09 dex) is slightly larger than expected on the basis of our error analysis (0.075 dex); the scatter for Fe II is larger, but in good agreement with expectations based on our error analysis. While this difference is not significant, given the small number of stars, it is possible that stars #7004050 and #7004487 are indeed slightly

more metal-poor (by about 0.15 dex) than the average of the remaining three cluster members. It is also worth mentioning that star #7004050 is also slightly bluer than the other member stars of NGC 6441, by about 0.08 mag in the $V - I$ color: this is roughly the color difference expected for the metallicity difference found in our analysis. More data on a wider sample of stars of NGC 6441 are clearly required to definitely set the issue about an intrinsic spread in metal abundances in this cluster.

To our knowledge, this is the first determination of the metal abundance of NGC 6441 from high dispersion spectra of individual stars. We found in the literature only three previous metallicity determinations for NGC 6441. The first two are based on integrated light. Zinn & West (1984) used the Q39 index to obtain a metallicity of $[\text{Fe}/\text{H}] = -0.59 \pm 0.15$. A somewhat higher metallicity of $[\text{Fe}/\text{H}] = -0.47 \pm 0.12$ dex was obtained by Armandroff & Zinn (1988) from spectroscopy of the Ca II IR triplet, calibrated on the Zinn & West scale. Armandroff and Zinn averaged these two values to produce the value of $[\text{Fe}/\text{H}] = -0.53 \pm 0.11$. That is listed by Harris (1996) and usually adopted in the discussion of this cluster. Very recently, Clementini et al. (2005) have measured metal abundances for a few RR Lyrae in NGC 6441 using a variant of the ΔS method, obtaining $[\text{Fe}/\text{H}] = -0.69 \pm 0.06$ on the Zinn & West scale, and $[\text{Fe}/\text{H}] = -0.41 \pm 0.06$ on the Carretta & Gratton (1997) scale, with a quite considerable star-to-star scatter of more than 0.3 dex (*r.m.s.*). The present metal abundance should be compared with that on the Carretta & Gratton scale, which is based on an analysis method quite consistent with that here considered. Indeed, this last comparison is quite good. Finally, we note that if we add the point of NGC 6441 to the correlation between abundances from high dispersion spectra by our group (see Carretta et al. 2001) and those by Zinn & West (1984), a linear relationship between the two scales would be favored, rather than a cubic one as considered by Carretta et al. (2001).

4.4. Abundances for other elements

Table 8 lists the abundances for the individual elements for stars member of NGC 6441, while Table 9 is for field stars. For each star and element, we give the number of lines used in the analysis, the average abundance, and the *r.m.s.* scatter of individual values. The Na abundances include corrections for departures from LTE, following the treatment by Gratton et al. (1999). Abundances for the odd elements of the Fe group (Sc, V, and Mn) were derived with consideration for the not negligible hyperfine structure of these lines (see Gratton et al. 2003 for more details). Finally, we note that telluric absorption lines were removed from the spectra in the region around the [OI] lines. No attempt was made to remove the strong auroral emission line; however, due to the combination of the Earth and stellar motions at the epoch of observations, the auroral emission line typically is about 0.7 Å blueward to

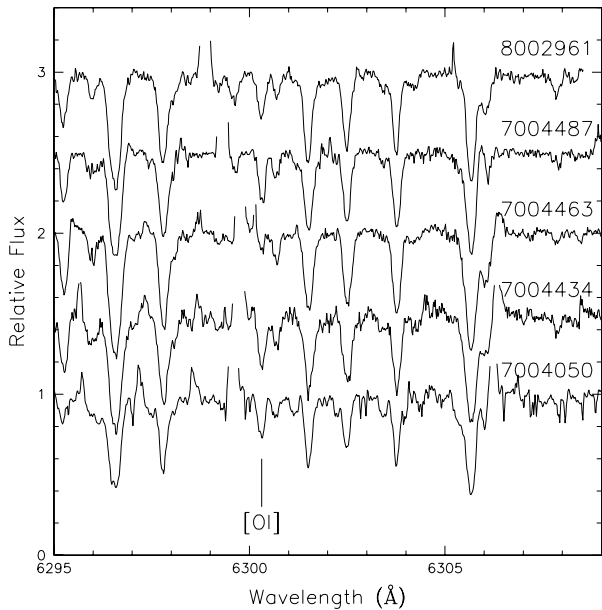


Fig. 2. Spectral region including the [OI] line at 6300.3 Å for the member stars of NGC 6441. The spectra have been corrected for the individual radial velocities and offset vertically for clarity

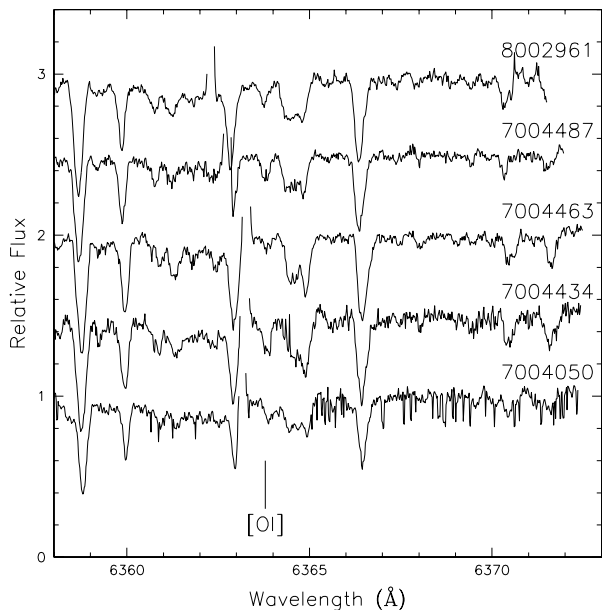


Fig. 3. Spectral region including the [OI] line at 6363.8 Å for the member stars of NGC 6441. The spectra have been corrected for the individual radial velocities and offset vertically for clarity

the stellar line, so that it does not create problems at the resolution of the UVES spectra. The O abundances were derived from equivalent widths: however, they were later confirmed by spectral synthesis. We did not apply any correction for the blending with the Ni I line at 6300.339 Å,

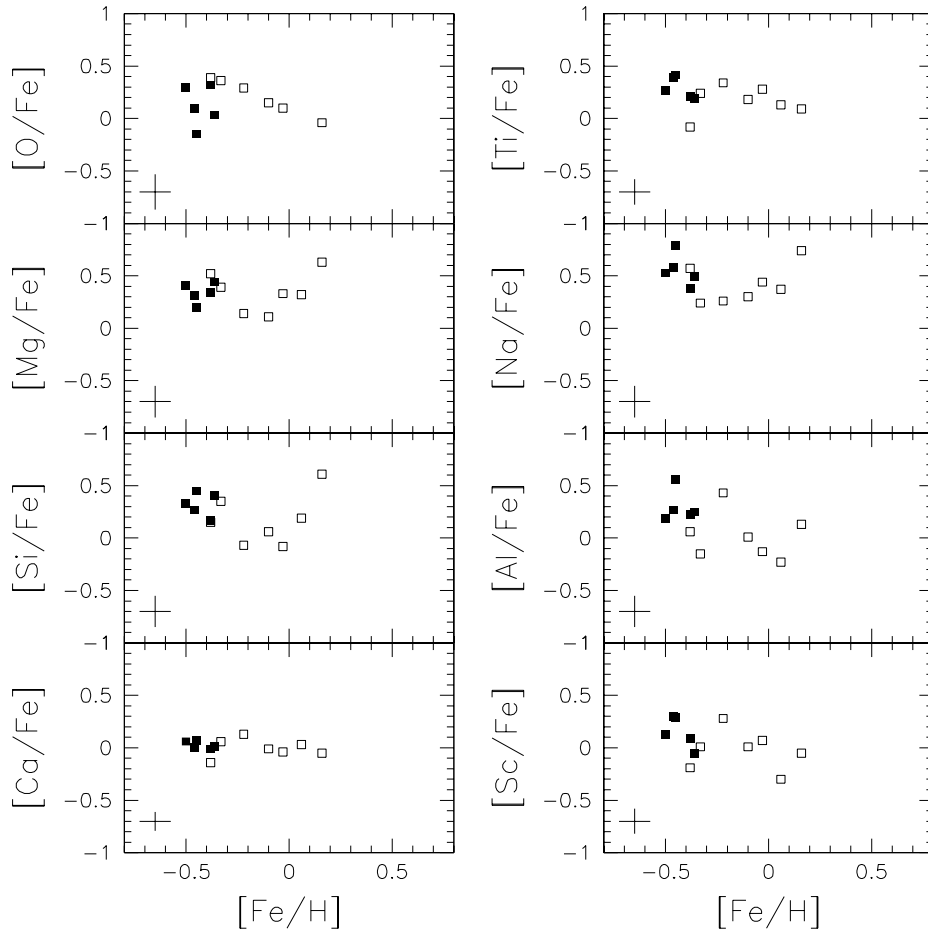


Fig. 6. Run of abundance ratios versus metallicity $[\text{Fe}/\text{H}]$ for the analyzed stars. Filled symbols are stars member of NGC 6441; open symbols are field stars. Error bars are at bottom left of each panel. On the left, from top to bottom: $[\text{O}/\text{Fe}]$, $[\text{Mg}/\text{Fe}]$, $[\text{Si}/\text{Fe}]$, and $[\text{Ca}/\text{Fe}]$. On the right, from top to bottom: $[\text{Ti}/\text{Fe}]$ (from neutral lines alone), $[\text{Na}/\text{Fe}]$, $[\text{Al}/\text{Fe}]$, and $[\text{Sc}/\text{Fe}]$

nor for formation of CO. The blending Ni I line is expected to contribute about 4 mÅ to the EW of the [OI] line, using the line parameters by Allende Prieto et al. (2001); this corresponds to correcting the O abundances about 0.05 dex downward. CO coupling should be strong at the low effective temperature of the program stars. Unluckily, the abundance of C is not determined. However, we expect that C is strongly depleted in stars near the tip of the red giant branch, with expected values of $[\text{C}/\text{Fe}] \sim -0.6$ (Gratton et al. 2000). If the original C abundance in unevolved stars follows the Fe one (as usually observed in metal-rich environments: see e.g. Gratton et al. 2000), then we expect typical values of $[\text{C}/\text{O}] \sim -0.8$ for stars in NGC 6441. Neglecting CO formation, we should have underestimated the O abundances from forbidden lines by ~ 0.05 dex. These two corrections should roughly compensate, however, they both are within the error bars of the present determinations.

The last two columns of Table 8 give the average abundance for the cluster, as well as the *r.m.s.* scatter of individual values around this mean value. In general, the values for the scatter agree fairly well with those estimated

in our error analysis. Large scatters are however determined for the light elements O, Na, Mg, and Al; the elements participating in the so-called Na-O anticorrelation. Inspection of Table 8 reveals that while four stars share a similar composition (high O and Mg abundances, low Na and Al ones), one star (#7004463) has much lower O and Mg abundances, and higher Na and Al ones. Figures 2, 3, and 4 show the spectral region around the two [OI] lines and the Na doublet at 6154-60 Å in the spectra of the stars of NGC 6441. The weakness of the [OI] lines and the strength of the Na doublet in the spectrum of star #7004463 is quite obvious (note that the five stars have all similar temperatures and reddenings). This star seems a typical representative of the O-poor, Na-rich stars often found among Globular cluster stars. Figure 5 shows the O-Na and Mg-Al anticorrelations from our data set. The curve plotted in the upper panel is from Fig. 5 in Carretta et al. (2006) and indicates the typical behavior of $[\text{O}/\text{Fe}]$ with respect to $[\text{Na}/\text{Fe}]$ as defined by a collection of stars in about 20 Globular clusters. More extensive data about the O-Na anticorrelation among stars in NGC 6441 will be

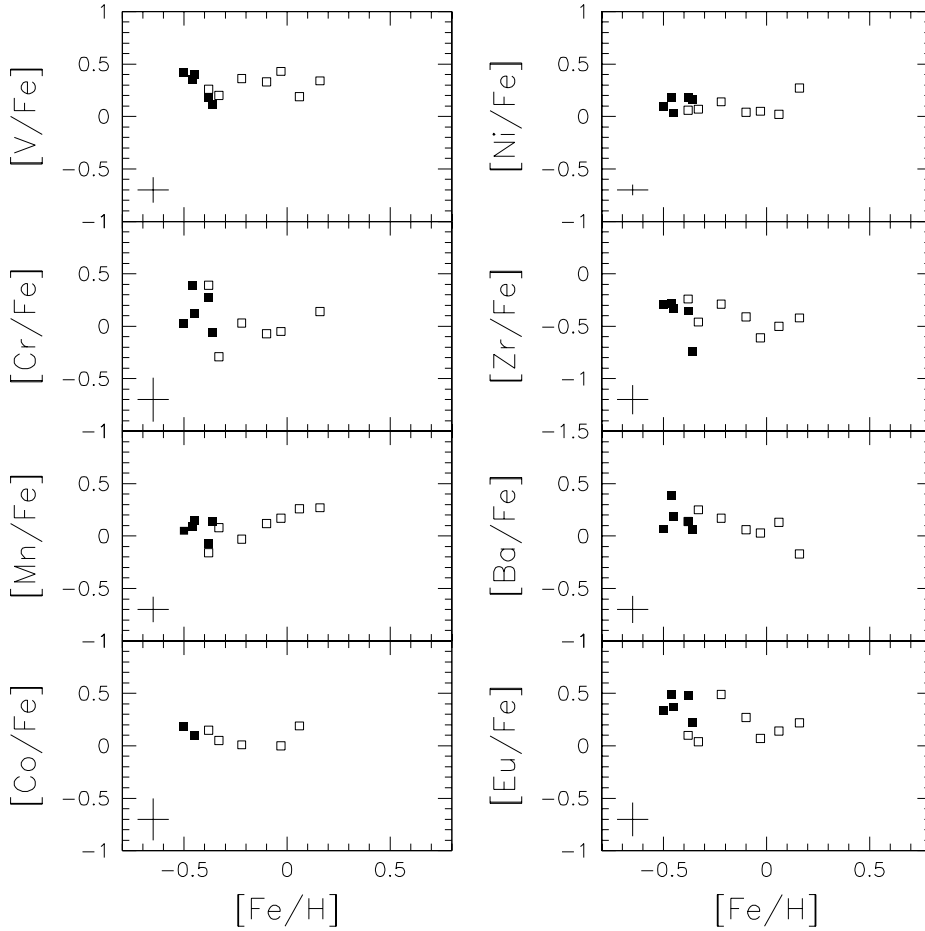


Fig. 7. Run of abundance ratios versus metallicity $[\text{Fe}/\text{H}]$ for the analyzed stars. Filled symbols are stars member of NGC 6441; open symbols are field stars. Error bars are at bottom left of each panel. On the left, from top to bottom: $[\text{V}/\text{Fe}]$, $[\text{Cr}/\text{Fe}]$, $[\text{Mn}/\text{Fe}]$, and $[\text{Co}/\text{Fe}]$. On the right, from top to bottom: $[\text{Ni}/\text{Fe}]$, $[\text{Zr}/\text{Fe}]$, $[\text{Ba}/\text{Fe}]$, and $[\text{Eu}/\text{Fe}]$

discussed separately, on the basis of the GIRAFFE spectra taken simultaneously with the UVES ones.

4.5. Comparison between NGC 6441 and the field stars

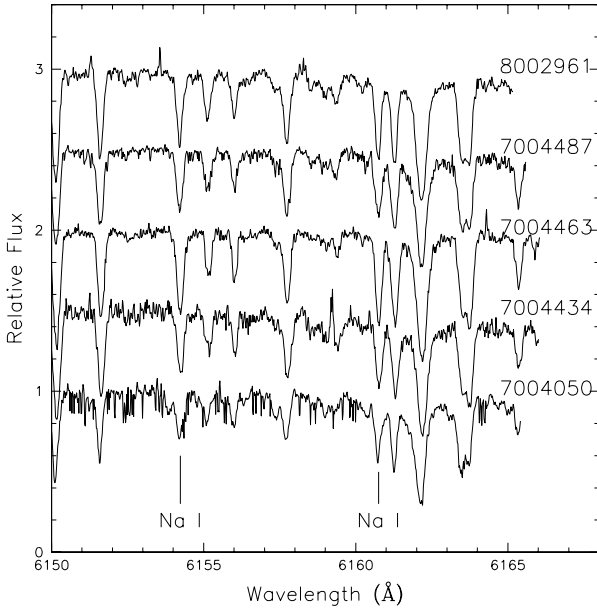
The runs of the abundance ratios with respect to Fe are plotted against metal abundances in Figures 6 and 7. In these plots, filled symbols are for member stars of NGC 6441, while open symbols are for field stars. These figures highlight that the field stars are a quite heterogeneous group. Three stars (#6003734, 7005308, and 8003092) are moderately metal-poor, with a metal abundance only slightly larger than that of NGC 6441. They have a composition quite similar to that of the cluster, though the last one has a smaller excess of Si. The two first stars have rather large absolute values of the radial velocities: this suggests that they are old, the excess of Oxygen and α -elements being possibly due to a reduced contribution by type-Ia SNe. Three other stars (#7005341, 7004329, and 7004453) have almost solar abundances. They have a low absolute value of the radial velocity. Finally, star #7004360 has a peculiar, high metal content. Our analy-

sis yielded a significant excess of the α -elements Mg and Si, but not of O, Ca, and Ti; also Na is overabundant, but not Al. However, given the difficulties related to the analysis of this spectrum, extremely line rich, we prefer not to comment any more on this star.

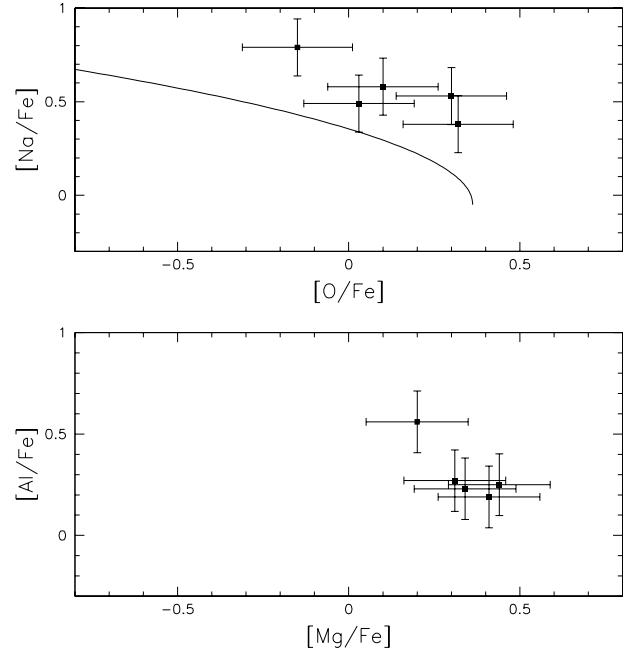
Comparison between field (likely bulge) and cluster stars may be interesting and meaningful, because most of the analysis concerns are reduced. In particular, deficiencies of model atmospheres or departures from LTE are expected to act similarly in stars having similar atmospheres. We may for instance compare the stars of NGC 6441 with the group of the field "metal-poor" stars, that have similar overall metal abundances (see Table 10). The two sets of stars display a quite similar pattern of abundances, both characterized by an excess of α -elements; also the apparent deficiency of Ca, Y, and Zr is similar. On this respect we notice that the three field stars (likely bulge) display similar Ca abundances ($[\text{Ca}/\text{Fe}] \sim -0.2$), and similar abundances for Y ($[\text{Y}/\text{Fe}] \sim -0.5$) and Zr ($[\text{Zr}/\text{Fe}] \sim -0.8$), suggesting that the low Ca, Y and Zr abundances are artifacts of the analysis, rather than real features of these stars. We notice that the present analy-

Table 8. Abundances for NGC 6441 members

Element	7004050			7004434			7004463			7004487			8002961			Cluster Average	<i>r.m.s.</i>
	N	mean	<i>r.m.s.</i>														
[Fe/H]	53	-0.46	0.19	54	-0.38	0.23	59	-0.45	0.18	53	-0.50	0.13	59	-0.36	0.15	-0.43	0.06
[O/Fe]I	2	+0.10	0.08	2	+0.32	0.11	1	-0.15		2	+0.30	0.14	2	+0.03	0.04	+0.12	0.20
[Na/Fe]I	2	+0.58	0.08	2	+0.38	0.10	2	+0.79	0.10	2	+0.53	0.00	2	+0.49	0.08	+0.55	0.15
[Mg/Fe]I	2	+0.31	0.01	2	+0.34	0.06	2	+0.20	0.02	2	+0.41	0.09	2	+0.44	0.08	+0.34	0.09
[Al/Fe]I	2	+0.27	0.08	2	+0.23	0.15	2	+0.56	0.23	2	+0.19	0.16	2	+0.25	0.21	+0.30	0.15
[Si/Fe]I	1	+0.27		2	+0.17	0.09	2	+0.45	0.17	3	+0.33	0.06	2	+0.41	0.16	+0.33	0.11
[Ca/Fe]I	12	0.00	0.19	11	-0.01	0.20	10	+0.07	0.15	12	+0.06	0.22	12	+0.01	0.16	+0.03	0.04
[Sc/Fe]II	3	+0.30	0.24	3	+0.09	0.12	3	+0.29	0.20	3	+0.13	0.07	3	-0.05	0.09	+0.15	0.15
[Ti/Fe]I	5	+0.39	0.09	6	+0.21	0.21	6	+0.41	0.18	6	+0.27	0.11	7	+0.19	0.15	+0.29	0.10
[Ti/Fe]II	1	+0.50		1	+0.34		1	+0.18		1	+0.18		1	+0.43		+0.33	0.14
[V/Fe]I	9	+0.35	0.17	15	+0.18	0.18	14	+0.40	0.17	12	+0.42	0.15	11	+0.11	0.14	+0.29	0.14
[Cr/Fe]I	1	+0.39		1	+0.27		1	+0.12		1	+0.03		1	-0.06		+0.15	0.18
[Mn/Fe]I	3	+0.09	0.19	3	-0.07	0.13	3	+0.15	0.20	3	+0.05	0.18	3	+0.14	0.12	+0.07	0.09
[Ni/Fe]I	21	+0.18	0.16	23	+0.18	0.17	23	+0.03	0.20	25	+0.09	0.20	24	+0.16	0.14	+0.13	0.07
[Y/Fe]I	1	-0.34		1	+0.01		1	+0.31		1	-0.11		1	-0.10		-0.05	0.24
[Zr/Fe]I	4	-0.28	0.28	5	-0.35	0.20	5	-0.33	0.18	5	-0.29	0.22	5	-0.74	0.11	-0.40	0.19
[Ba/Fe]II	3	+0.39	0.21	3	+0.14	0.15	3	+0.19	0.18	3	+0.07	0.08	3	+0.06	0.18	+0.17	0.13
[Eu/Fe]II	1	+0.49		2	+0.48	0.03	2	+0.37	0.07	2	+0.34	0.19	2	+0.22	0.04	+0.32	0.11

**Fig. 4.** Spectral region including the Na I doublet at 6154–60 Å for the member stars of NGC 6441. The spectra have been corrected for the individual radial velocities and offset vertically for clarity

sis makes the same assumptions of Gratton et al. (2003), where we did not find a similar low Ca abundance in (local) metal-rich dwarfs. It seems more likely that the problem is limited to the analysis of bright giants. All Ca lines used here are strong, with $EWs \geq 100$ mÅ. They form at tiny optical depths, and are potentially sensitive to details of the model atmospheres as well as to departures from LTE. However, the differential comparison with the non metal rich bulge stars suggests that NGC 6441 and the field metal-poor stars considered in this analysis have a small but clear excess of Ca, and roughly normal abundances of Y and Zr.

**Fig. 5.** Upper Panel: [Na/Fe] ratio as a function of [O/Fe], for stars member of NGC 6441, the curve indicates the mean [O/Fe] vs [Na/Fe] locus for a collection of ~ 20 Globular clusters (Carretta et al. 2006). Lower panel: [Al/Fe] ratio as a function of [Mg/Fe], for the same stars.

The main difference between the stars of NGC 6441 and the field moderately metal-poor stars, concerns the elements involved in the p-capture process of O, Na, Mg, and Al. Even leaving aside the obvious case of the O-poor, Na-rich star #7004463, the stars of NGC 6441 are systematically more O and Mg poor, and Na and Al rich than the similar field stars. This suggests that even the more normal star might have been somewhat polluted by material processed through H-burning at high temperature. This is well confirmed by a comparison of the [O/Na] abundance ratios in NGC 6441 with those typical of other

Table 9. Abundances for field stars

Element	6003734			7004360			7005308			7005341		
	N	mean	<i>r.m.s.</i>									
[Fe/H]	62	-0.33	0.18	44	+0.16	0.17	64	-0.22	0.21	62	-0.03	0.23
[O/Fe]I	2	+0.36	0.01	2	-0.04	0.15	2	+0.22	0.15	1	+0.10	
[Na/Fe]I	2	+0.24	0.13	2	+0.74	0.19	2	+0.26	0.28	2	+0.44	0.10
[Mg/Fe]I	2	+0.39	0.13	2	+0.63	0.17	2	+0.14	0.34	2	+0.33	0.12
[Al/Fe]I	2	-0.15	0.12	2	+0.13	0.17	2	+0.43	0.01	2	-0.13	0.21
[Si/Fe]I	2	+0.35	0.16	3	+0.61	0.20	2	-0.07	0.29	2	-0.08	0.20
[Ca/Fe]I	13	-0.06	0.19	13	-0.05	0.17	11	+0.13	0.17	11	-0.04	0.23
[Sc/Fe]II	2	+0.01	0.12	3	-0.05	0.32	2	+0.28	0.19	3	+0.07	0.46
[Ti/Fe]I	7	+0.24	0.20	6	+0.09	0.14	7	+0.34	0.17	6	+0.28	0.06
[Ti/Fe]II	1	-0.08		1	+0.39		1	-0.02		1	+0.04	
[V/Fe]I	10	+0.20	0.16	11	+0.34	0.16	15	+0.36	0.17	15	+0.43	0.22
[Cr/Fe]I	1	-0.29		1	+0.14		1	+0.03		1	-0.05	
[Mn/Fe]I	3	+0.08	0.13	3	+0.27	0.11	3	-0.03	0.07	3	+0.17	0.11
[Co/Fe]I	1	+0.05					1	+0.01		1	0.00	
[Ni/Fe]I	25	+0.07	0.19	24	+0.27	0.19	24	+0.14	0.19	25	+0.05	0.25
[Y/Fe]I	1	-0.23		1	+0.42		1	-0.23		1	-0.31	
[Zr/Fe]I	5	-0.46	0.20	4	-0.42	0.24	3	-0.29	0.09	4	-0.61	0.17
[Ba/Fe]II	2	+0.25	0.13	3	-0.17	0.30	3	+0.17	0.13	3	+0.03	0.13
[Eu/Fe]II	1	+0.04		2	+0.22	0.10	2	+0.49	0.09	2	+0.07	0.07
Element	7004329			7004453			8003092					
	N	mean	<i>r.m.s.</i>	N	mean	<i>r.m.s.</i>	N	mean	<i>r.m.s.</i>			
[Fe/H]	58	+0.06	0.16	64	-0.10	0.20	48	-0.38	0.23			
[O/Fe]I				2	+0.15	0.10	2	+0.39	0.07			
[Na/Fe]I	2	+0.37	0.00	2	+0.30	0.15	2	+0.57	0.23			
[Mg/Fe]I	2	+0.32	0.05	2	+0.11	0.02	2	+0.52	0.05			
[Al/Fe]I	2	-0.23	0.25	2	-0.01	0.20	2	+0.06	0.17			
[Si/Fe]I	2	+0.19	0.06	2	+0.06	0.10	2	+0.15	0.17			
[Ca/Fe]I	11	-0.03	0.15	11	-0.01	0.17	10	-0.14	0.23			
[Sc/Fe]II	3	-0.30	0.23	3	+0.01	0.20	3	-0.19	0.24			
[Ti/Fe]I	6	-0.13	0.18	7	-0.18	0.13	5	-0.08	0.28			
[Ti/Fe]II	1	-0.02		1	+0.33		1	+0.14				
[V/Fe]I	14	+0.19	0.17	14	+0.33	0.20	12	+0.26	0.20			
[Cr/Fe]I				1	-0.07		1	+0.39				
[Mn/Fe]I	3	+0.26	0.15	3	+0.12	0.16	3	-0.16	0.14			
[Co/Fe]I	1	+0.19					1	+0.15				
[Ni/Fe]I	24	+0.02	0.12	24	+0.04	0.17	20	+0.06	0.23			
[Y/Fe]I	1	-0.31		1	+0.03		1	-0.31				
[Zr/Fe]I	4	-0.50	0.20	4	-0.41	0.14	4	-0.24	0.22			
[Ba/Fe]II	3	+0.13	0.22	3	+0.06	0.18	3	+0.14	0.21			
[Eu/Fe]II	2	+0.14	0.22	2	+0.27	0.06	2	+0.10	0.07			

Globular cluster stars (see Fig. 5 in Carretta et al. 2006). The other analyzed elements appear much more similar between NGC 6441 and the moderately metal-poor field stars, although the abundance ratios to Fe are generally higher in the stars of NGC 6441 by about 0.05-0.1 dex, which might be explained collectively by assuming some difference in Fe. This might suggest the existence of some subtle difference in the nucleosynthesis, although this result is at the limit of the observational and analysis uncertainty, and we do not give much weight to it.

Among the n-capture elements, stars in NGC 6441 have [Ba/Fe] abundance ratios similar to that of field stars; the [Eu/Fe] abundance ratios are on average larger than the putative metal rich bulge stars (by about 0.2 dex).

The larger [Eu/Ba] ratios may be again explained as due to larger contributions by core collapse SNe.

4.6. Comparison with other bulge objects

Comparisons with abundances from the literature must be considered with more caution, due to possible systematic differences in the analysis. In Table 10 we give average abundances for two other bulge clusters analyzed with a similar method (NGC 6528: Carretta et al. 2001; NGC 6553: Cohen et al. 1999), Baade's Window (McWilliam & Rich 1994), and for the cluster Terzan 7, likely belonging to the Sagittarius Dwarf Galaxy (Sbordone et al. 2005). The pattern of abundances seen in the various bulge clusters is quite similar. The main differences concern: (i)

Table 10. Mean Abundances in Clusters and Group of Stars

Element	NGC 6441		Metal-poor		Metal-Rich		NGC 6528		NGC 6553		Baade		Terzan 7	
	(1)		(1)		(1)		(2)		(3)		Window (4)		(5)	
	mean	<i>r.m.s.</i>	mean	<i>r.m.s.</i>	mean	<i>r.m.s.</i>	mean	<i>r.m.s.</i>	mean	<i>r.m.s.</i>	mean	<i>r.m.s.</i>	mean	<i>r.m.s.</i>
[Fe/H]	-0.43	0.08	-0.31	0.08	-0.02	0.08	+0.07	0.02	-0.16	0.08	-0.33		-0.59	0.07
[O/Fe] _I	+0.14	0.20	+0.32	0.09	+0.13	0.04	+0.07	0.11	+0.50	0.13	+0.03	0.18		
[Na/Fe] _I	+0.46	0.18	+0.22	0.17	+0.27	0.07	+0.40	0.12			+0.21	0.37		
[Mg/Fe] _I	+0.34	0.09	+0.35	0.19	+0.25	0.12	+0.14	0.09	+0.41	0.10	+0.35	0.14	-0.11	0.07
[Al/Fe] _I	+0.30	0.15	+0.11	0.29	-0.12	0.12								
[Si/Fe] _I	+0.33	0.11	+0.14	0.21	+0.06	0.14	+0.36	0.07	+0.14	0.18	+0.18	0.24	+0.07	0.09
[Ca/Fe] _I	+0.03	0.04	+0.02	0.14	-0.01	0.04	+0.23	0.06	+0.26	0.09	+0.14	0.17	0.00	0.14
[Sc/Fe] _{II}	+0.15	0.15	+0.03	0.24	-0.07	0.20	-0.05	0.10	-0.12	0.18	+0.29	0.20		
[Ti/Fe] _I	+0.29	0.10	+0.17	0.22	+0.20	0.08	+0.03	0.07	+0.19	0.06	+0.34	0.10	-0.05	0.07
[Ti/Fe] _{II}	+0.33	0.14	+0.01	0.11	+0.12	0.19								
[V/Fe] _I	+0.29	0.14	+0.27	0.08	+0.32	0.12	-0.20	0.09			+0.06	0.19		
[Cr/Fe] _I	+0.15	0.18	+0.04	0.34	-0.06	0.01	0.00	0.04	+0.04	0.09	-0.04	0.19		
[Mn/Fe] _I	+0.07	0.09	-0.04	0.12	+0.18	0.07	-0.37	0.07						
[Co/Fe] _I	+0.14	0.07	+0.07	0.07	+0.10	0.13								
[Ni/Fe] _I	+0.13	0.07	+0.09	0.04	+0.04	0.02	+0.10	0.05	+0.01	0.07	-0.04	0.08	-0.19	0.05
[Y/Fe] _I	-0.05	0.24	-0.26	0.05	-0.20	0.20								
[Zr/Fe] _I	-0.40	0.19	-0.33	0.12	-0.51	0.10								
[Ba/Fe] _{II}	+0.17	0.13	+0.19	0.06	+0.07	0.05	+0.14	0.07			+0.20	0.28		
[Eu/Fe] _{II}	+0.38	0.11	+0.21	0.24	+0.16	0.10								

(1) This paper

(2) Carretta et al. (2001)

(3) Cohen et al. (1999)

(4) McWilliam & Rich (1994)

(5) Sbordone et al. (2005)

the light elements involved in the p-capture processes (O, Na, and Mg). However, they may result from small number statistics, given the large star-to-star spread observed within each cluster. (ii) Ca, for which we think our abundance is not representative of the cluster real abundance (the stars discussed here are much cooler than those analyzed in NGC 6528 and NGC 6553). (iii) Mn, for which we derive a nearly solar ratio to Fe in NGC 6441, while Carretta et al. derived a low abundance in NGC 6528. This difference in Mn abundance might indicate a different chemical history. Mn is known to be under-abundant in quite metal-rich stars of the Sagittarius dwarf spheroidal (McWilliam et al. 2003); however the composition of NGC 6528 (and NGC 6441) is also clearly different from that of Terzan 7 and other stars in the Sagittarius Dwarf Galaxy, since in these last cases the α -elements are not at all overabundant. All these facts suggest that various bulge clusters had different chemical histories, possibly being originated in different fragments of our Galaxy.

5. Conclusion

This paper presents the first high resolution spectroscopic analysis of individual NGC 6441 stars. A total of thirteen RGB stars were observed using FLAMES/UVES, only five of them, on the basis of their measured radial velocities, positions and chemical compositions are very likely members of NGC 6441. The iron abundance measured for the cluster stars is $[\text{Fe}/\text{H}] = -0.39 \pm 0.04 \pm 0.05$ dex, somewhat

higher than those reported in the literature (see e.g. Zinn & West 1984 and Armandroff & Zinn, 1988) which are however based on lower resolution data. In a more recent paper, Clementini et al. (2005) measured the metal abundance of NGC 6441 RR Lyrae stars finding an average metallicity of $[\text{Fe}/\text{H}] = -0.41 \pm 0.06$ dex which is perfectly consistent with our results.

Some of the results obtained seem to hint that NGC 6441 was characterized by slightly different nucleosynthetic processes. In fact, in the cluster stars O and Mg are systematically lower and Na and Al higher than in the field stars, and the $[\text{O}/\text{Na}]$ ratios measured in NGC 6441 are different from those typical of other clusters.

We find a very small metallicity spread among the stars in our sample which belong to the cluster, only marginally larger than the level expected on the basis of the observational error, suggesting an homogeneous composition. However, our sample is far too small to be representative of the cluster distribution and, on the other hand, Clementini et al. (2005), find a scatter as high as 0.3 dex. The derived homogeneity could be just due to limited sampling and thus no definite conclusion can be drawn on the basis of the present data. The GIRAFFE/FLAMES data presented by Gratton et al. (2006 in preparation) as well as the near-IR NIRSPEC ones in Origlia et al. (2006 in preparation) will hopefully address this issue.

Acknowledgements. We wish to thank our anonymous referee for his/her comments and suggestions. This research has

been funded by PRIN 2003029437 "Continuità e discontinuità nella formazione della nostra Galassia" by the Italian MIUR. This publication makes use of data products from the Two Micron All Sky Survey, which is a joint project of the University of Massachusetts and the Infrared Processing and Analysis Center/California Institute of Technology, funded by the National Aeronautics and Space Administration and the National Science Foundation

References

- Allende Prieto, C., Lambert, D.L., & Asplund, M. 2001, *ApJL*, 556, L63
- Alonso, A., Arribas, S. & Martinez-Roger, C. 1999 *A&AS*, 140, 261
- Armandroff, T., & Zinn, R. 1988, *AJ*, 96, 92
- Bedin, L.R., Piotto, G., Anderson J., et al. 2004, *ApJ*, 605, 125
- Barklem, P.S., Piskunov, N., O'Mara, B.J. 2000, *A&AS*, 142, 467
- Bragaglia, A., et al. 2001, *A&A*, 121, 327
- Cardelli, J.A., Clayton, G.C., & Mathis, J.S. 1989, *ApJ*, 345, 245
- Carretta, E., & Gratton, R.G. 1997, *A&AS*, 121, 95
- Carretta, E., Cohen, J.G., Gratton, R.G., & Behr, B.B. 2001, *AJ*, 122, 1469
- Carretta, E., Bragaglia, A., Gratton, R.G., et al. 2006, *A&A* accepted (astro-ph/0511833)
- Cayrel, R. 1988, in *The Impact of Very High S/N Spectroscopy on Stellar Physics*, IAU Symp. 132, ed. G. Cayrel de Strobel & M. Spite, Kluwer Academic Publishers, Dordrecht, p.345
- Clementini, G., Gratton, R.G., Bragaglia, A., et al. 2005, *A&A*, in press (astro-ph/0508079)
- Cohen, J.G., Gratton, R.G., Behr, B.B., & Carretta, E. 1999, *ApJ*, 523, 739
- Cutri, R.M., et al. 2003, *VizieR On-line Data Catalog: II/246*. Originally published in: University of Massachusetts and Infrared Processing and Analysis Center, (IPAC/California Institute of Technology)
- D'Antona, F., & Caloi, V. 2004, *ApJ*, 611, 871
- Dubath, P., Meylan, G., & Mayor, M. 1997, *A&A*, 324, 505
- Ferraro, F. R., Beccari, G., Rood, R. T., Bellazzini, M., Sills, A., Sabbi, E. 2004, *AJ*, 603, 127
- Gratton, R.G. 1988, *Rome Obs. Preprint*, 29
- Gratton, R.G., Carretta, E., Eriksson, K., & Gustafsson, B., 1999, *A&A*, 350, 955
- Gratton, R.G., Sneden, C., Carretta, E., & Bragaglia, A., 2000, *A&A*, 354, 169
- Gratton, R.G., Carretta, E., Claudi, R., Lucatello, S., & Barbieri, M. 2003, *A&A*, 408, 529
- Gratton, R.G., Sneden, C., & Carretta, E., 2004, *ARA&A*, 42, 385
- Harris, W.E. 1996, *AJ*, 112, 1487
- Kurucz, R.L. 1992, in *The Stellar Populations of Galaxies*, IAU Symp. 149, B. Barbuy & A. Renzini eds, Kluwer Academic Publishers, Dordrecht, p.225
- Layden, A.C., Ritter, L.A., Welch, D.L., & Webb, T.M.A. 1999, *AJ*, 117, 1313
- Magain, P., 1984, *A&A*, 134, 189
- Manfroid, J., Selman, F. & Jones, H. 2001, *The Messenger*, 104,16
- McWilliam, A. & Rich, R.M. 1994, *ApJS*, 91, 749
- McWilliam, A., Rich, R.M., & Smecker-Hane, T.A. 2003, *ApJ*, 592, 21
- Momany, Y., Bedin, L. R., Cassisi, S., Piotto, G., Ortolani, S., Recio-Blanco, A., De Angeli, F., & Castelli, F. 2004, *A&A*, 420, 605
- Momany, Y., Held, E. V., Saviane, I., & Rizzi, L. 2002, *A&A*, 384, 393
- Pasquini, L. et al. 2002, *Messenger*, 110, 1
- Piotto, G., et al. 1997, in *Advances in Stellar Evolution*, ed. R. T. Rood & A. Renzini (Cambridge: Cambridge Univ. Press), 84
- Piotto, G., Villanova, S., Bedin, L.R., et al. 2005, *ApJ*, 621, 777
- Pritzl, B.J., Smith, H.A., Catelan, M., & Sweigart, A.V. 2001, *AJ*, 122, 2600
- Rich, R.M., Sosin, C., Djorgovski, S.G. et al. 1997, *ApJ*, 484, 25
- Sbordone, L., Bonifacio, P., Marconi, G., Buonanno, R., & Zaggia, S. 2005, *A&A*, 437, 905
- Schlegel, D.J., Finkbeiner, D.P., & Davis, M. 1998, *ApJ*, 500, 525
- Stetson, P. B. 1994, *PASP*, 106, 250
- Sweigart, A.V., 2001, in *Highlights Astron.*, 12, 292 (astro-ph/0103133)
- Sweigart, A.V., & Catelan, M. 1998, *ApJL*, 501, L63
- Valenti et al. 2006 in preparation
- Zinn, R., & West, M.J. 1984, *ApJS*, 55, 45